AD-767 415

ULTRA-WIDEBAND THIN FILM MODULATORS FOR CO_2 LASERS

P. K. Cheo, et al

United Aircraft Research Laboratories

Prepared for:

Office of Naval Research
Advanced Research Projects Agency

30 September 1973

ULTRA-WIDEBAND THIN FILM MODULATORS FOR CO_2 LASERS

SEMI-ANNUAL TECHNICAL REPORT

Period Covered: 25 March 1973 to 25 September 1973

Contract No. N00014-73-C-0087

Sponsored by

Advanced Research Projects Agency

ARPA Order No. 1860, Amendment No. 6

United Aircraft
Research Laboratories

UNITED AIRCRAFT CORPORATION

EAST HARTFORD, CONNECTICUT 06108

M921513-4

Semi-Annual Technical Report

Ultra-Wideband Thin Film Modulator for CO_2 Lasers

by

P. K. Cheo, M. Gilden, J. F. Black and J. L. Swindal
United Aircraft Research Laboratories
East Hartford, Connecticut 06108

September 30, 1973

Principle Investigator: P. K. Cheo (203) 565-4297

Prepared for the Office of Naval Research
Contracting Officer: Dr. M. White
Contract No. N00014-73-C-0087
Contractor Modification No. P00001 - $123,167.00
25 August 1972 to 25 December 1973

Sponsored by
Advanced Research Projects Agency
ARPA Order 1860, Amendment No. 9/11-15/72

Ultra-Wideband Thin Film Modulators for CO_2 Lasers

TABLE OF CONTENTS

1.0 TECHNICAL REPORT SUMMARY

1.1 Program Objectives

The long range objective of this program is to develop an efficient and practical ultra-wideband thin film modulator for CO_2 lasers useful for optical image radars and high-data-rate optical communication systems. During the present contracting period (25 May 1973 to 25 December 1973), the goal of this program is aimed at the demonstration of efficient sideband generation of a 10.6 μm CO_2 laser carrier at microwave frequencies (X-band) in a nonlinear GaAs thin film optical modulator element which is interfaced with a microwave ridge guide structure. Electrooptic interaction in a GaAs thin film between an optical guided-wave and either a traveling or a synchronous standing microwave signal can produce a sideband at the sum and difference frequencies. By using a frequency modulated microwave field, a chirped optical signal in the sideband is generated. This signal can be separated from others by a proper optical filtering technique such as a diffraction grating or a narrow bandpass interferometer. The development of such a device will be useful to provide the desired waveform from the master oscillator that will be employed in future high power CO_2 laser radar systems, and it will also have a great impact on future space optical communication systems where system design concepts change rapidly in accordance with new technological advances.

1.2 Method of Approach

Based on our past experiences (Refs. 1, 2, 3, 4 and 5) we believe that the replacement of active bulk devices for the modulation of 10 μm CO_2 lasers is not far away. This remarkable development is made possible by certain refinements in existing GaAs epitaxial thin film technology. In order to meet the goal of the present program, it is apparent that certain major areas of technology require immediate effort. They are: (1) the investigation of electrooptic properties of GaAs thin films suitable for phase modulation of 10.6 μm CO_2 laser radiation, (2) an improvement of optical coupling of a Gaussian beam into and out of a thin film optical waveguide and (3) the investigation of characteristics of two alternative microwave waveguide configurations with GaAs dielectric thin film loading. Using the knowledge and experience gained from the above described work, it is possible then to design and fabricate a thin film microwave modulator for 10.6 μm CO_2 laser radiation.

1.3 Technical Program Plan and Schedule

Basically this research program consists of four tasks. They are:

Task 1.0 - Phase Modulation Experiment

This initial experiment is a very important step of the program. It is designed to verify the fundamental principles underlying the basic approach of our proposed program to develop a thin film phase modulator. This task involves the design, fabrication, testing, and evaluation of a modified Mach Zehnder optical interferometer which contains two active elements. One of the elements is a beam splitter which is made of a Ge acoustooptic Bragg deflector, and the other is a GaAs thin film electrooptic modulator. A detailed discussion of this experiment will be given in Section 2.0.

Task 2.0 - Optical Waveguide Structures With Back-Scattered Grating Couplers

This task involves design, fabrication, testing and evaluation of several optical waveguide structures suitable for the study of optical couplers utilizing the backward excitation scheme (Ref. 6). Optical waveguide structures are fabricated from n/n^+, and $n/n^+/p^+$ GaAs epitaxial thin films as well as from Cr doped GaAs bulk crystal which is Bridgman grown material having very high resistivity ($\rho \gtrsim 10^8$ Ω-cm). Grating couplers consist of series parallel grooves etched into the GaAs thin film material by rf-sputtering. The desired grating pattern having a period $L \simeq 2.5$ μm is obtained by a standard photolithographic process. Grating couplers can be fabricated either on the surface of the thin film or at the interface between a substrate and an epi-layer. Detailed discussion on the fabrication techniques and some recent evaluation results of these couplers will be given in Section 3.0.

Task 3.0 - Microwave Ridge-Guide Structures With GaAs Thin Film Loading

This task involves the design, fabrication and study of the characteristics of a narrow gap ridge waveguide structure at microwave frequencies. Parameters investigated include the effective electrical impedance, attenuation coefficient, propagation constant and other circuit constants. Two alternative approaches; one an ordinary traveling wave structure and the other, a synchronous standing wave structure, are considered in this program. Details are given in Section 4.0.

Task 4.0 - Microwave Modulation Experiment

This task involves (1) an interfacing between an optical waveguide and a microwave ridge-guide, (2) generation and detection of sideband in thin films, and (3) investigation of the characteristics of the sideband signal. This experiment will be performed during the last quarter of this contractual period.

The program schedule is presented in Table I.

TABLE I – ARPA/ONR THIN FILM MODULATOR PROGRAM SCHEDULE

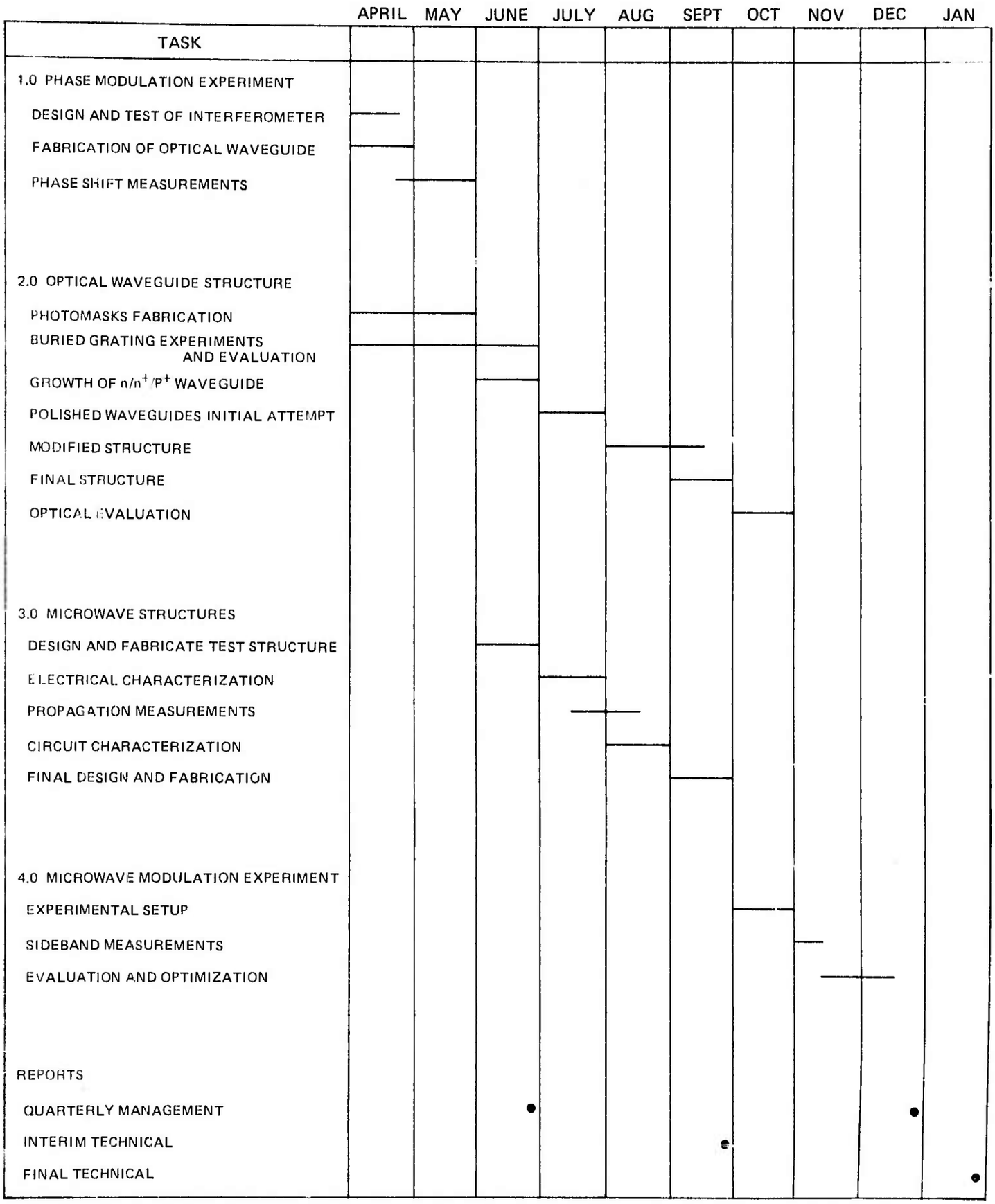

1.4 Major Accomplishments

Various tasks are progressing in accordance with the schedule. A number of accomplishments have been realized during this interim reporting period. They are:

A. Phase shift measurements of 10.6 μm guided wave modes in GaAs thin films have been made by a novel rf interferometric technique. This technique affords very accurate and convenient measurements of a phase-shift $\Delta\phi$ as a function of reverse-bias junction voltage. An improvement in measuring sensitivity greater than two orders of magnitude has been obtained with this technique over the conventional optical heterodyne and compensation techniques. Results of this experiment have been accepted for publication in Applied Physics Letters, Vol. 23, No. 8, 15 October 1973.

B. A number of photomasks for optical grating couplers with line spacings varied from 2.5 to 2.75 μm have been made with photo-reduction and step-repeat processes. These photomasks allow us to fabricate phase grating couplers suitable for the investigation of the characteristics of backward excitation of 10.6 μm guided-waves in GaAs thin films.

C. Attempts have been made to grow high resistivity, single crystal GaAs thin films on corrugated n^+ GaAs substrates by chemical vapor epitaxy. The periods of corrugation vary in the range from 2.5 to 3.5 μm. Gratings 3 mm square with etched grooves having a depth $\gtrsim 1.5$ μm were first formed in n^+ GaAs substrates. The high resistivity epitaxial layers were grown with controlled Cr doping to assure very low free carrier concentration ($N \leq 10^{12}/cm^3$). SEM results indicate that good single crystal GaAs thin films can be produced on corrugated substrates and that the quality of the epi-layer remains the same from the epi-surface all the way down to the substrate interface except for a narrow transition region (≤ 1 μm). The thickness of this transition region is a function of substrate preparation and epitaxial growth procedures.

D. A large effort has been made to determine the best optical waveguide configuration which meets the requirements for both the optical and microwave waveguides and can provide the optimum interfacing between the two structures. The selected configuration for fulfilling the goal of the present program objective is a 20 to 25 μm thick GaAs thin film obtained by chemo-mechanical polishing of a Bridgman grown, high resistivity, GaAs bulk crystal. Phase grating couplers are incorporated into this thin film which has been ruggedized by a layer of metallic film.

E. Several microwave ridge waveguide structures have been theoretically and experimentally analyzed. Microwave transmission experiments of these structures have been made. Measured results are in good agreement with our theoretical prediction and confirm our original design approach.

2.0 PHASE MODULATION EXPERIMENT

2.1 Introduction

This experiment is designed to verify the fundamental principle underlying the basic approach of the thin film wideband modulator program. More specifically, results of this experiment will provide an important test and evaluation of the thin film modulator materials and anomalies which may occur in nonlinear thin film materials. Since the goal of this program is to develop a thin film phase modulator by the generation of a sideband at the sum or difference frequencies of a CO_2 laser and a microwave modulated signal, it is necessary to demonstrate that phase modulation of a 10.6 μm laser carrier can be obtained by means of thin film materials.

2.2 Method of Approach

Phase shift measurements for the visible (Ref. 7) and the 1.15 μm (Ref. 8) lasers have been previously reported by using GaP p-n junctions and GaAs-Al_x-$Ga_{1-x}As$ double heterostructures as the electrooptically active medium. These measurements were made by means of either optical heterodyne and/or optical compensation methods (Ref. 9). They are measurements of interference fringes between two optical waves, whereby a very elaborate experimental setup and/or a complicated experimental procedure must be adopted in order to maintain extremely critical optical alignment and system stability. This requirement is well understood because the amount of phase-shift, as a result of two optical beams, varies with both the beam position and the optical path length to within a fraction of optical wavelength. This report (Ref. 3) describes a simple and novel measuring technique which provides accurate measurement of a small phase-shift ($\Delta\phi \sim 10^{o}$) and is considerably less sensitive to optical alignment. The basic idea is to measure the phase difference of two optical waves at a frequency where signal processing with extremely high discrimination and sensitivity can be achieved with the help of existing sophisticated rf electronic components.

2.3 Thin Film Modulator Structure

The structure of the thin film optical waveguide used in this work has previously (Ref. 1) been described in detail. It consisted of a high-resistivity ($\rho \geq 10^5$ Ω-cm) and low free carrier concentration ($N_f < 10^{13}$ cm^{-3}) GaAs thin film epitaxially grown on a heavily doped ($N_s > 10^{18}$ cm^{-3}) GaAs substrate. Included in this thin film modulator is a rectangular Schottky barrier electrode. At this doping level, the typical measured capacitance of the Schottky barrier junction is $\lesssim 0.3$ pF per one mm^2 electrode area at a 20 volt reverse-bias. The electrode is deposited on the surface of the epi-layer, and is located between two phase gratings with etched

grooves. These gratings, which are routinely made by standard microelectronic processes involving photolithographic and rf sputter-etch techniques described in detail in Section 3.0, are very convenient to use as input and output light couplers under proper phase matching conditions (Ref. 6).

2.4 Theory

Electrooptic phase modulation of a guided-wave mode in a thin film is to induce a maximum birefringence for the TE modes and minimum or zero birefringence for the TM modes propagating along a thin film of specific orientation. The phase change $\Delta\phi$ is directly proportional to the change of refractive index Δn of the waveguide as given by

$$\Delta\phi = \frac{2\pi}{\lambda} \ell \Delta n \tag{1}$$

where $\lambda = 10\ \mu m$, ℓ is the interaction length of the optical waveguide.

The change of refractive index Δn as a result of an external electric field can be obtained from the general equation (Ref. 10) of the indicatrix, relating the indices n_{ij} of a specific crystal orientation with the electric field components E_k through a linear electrooptic tensor r_{ijk}, as given by

$$\sum_{ijk} \left(\frac{1}{n_{ij}^2} + r_{ijk} E_k \right) x_i x_j = 1 \tag{2}$$

where i, j, k, run from 1 to 3. By the usual rule of contraction, the tensor components r_{ijk} can be expressed as r_{mk}, where m runs from 1 to 6. For a cubic crystal such as GaAs, there is only one electrooptic coefficient (r_{41}), and it can be shown that a field applied normal to one of the cubic axes always produces the maximum birefringence. In our expitaxial growth, the plane of the thin films is (100) and the field E is applied along the x_1 axis. For this case Eq. (2) reduces to

$$(x_1^2 + x_2^2 + x_3^2)/n^2 + 2\, r_{41}\, x_2 x_3 E = 1 \tag{3}$$

For a TE mode propagating along either the (011) axis (x_2') or the (01$\bar{1}$) axis (x_3'), a simple coordinate transformation shows that the change of index of refraction for a TE mode along x_2' is $+(n^3 r_{41} E)/2$ and along x_3' is $-(n^3 r_{41} E)/2$. There will be no change in index of refraction for the TM mode, as expected. Therefore Eq. (1) can be expressed as

$$\Delta\phi = \frac{2\pi}{\lambda} \ell \Delta n = \frac{\pi}{\lambda} \ell n^3 r_{41} \frac{V}{t} \tag{4}$$

where $r_{41} = 1.2 \times 10^{-10}$ cm/volt. V is the external voltage applied to the thin film and t is the thickness of the guide. Taking t = 20 μm and ℓ = 3 cm. The power converted into the sideband can be approximated by

$$\begin{aligned} E = E_o[J_o(\Delta\phi)\sin(\omega_o t + \phi_o)] \\ + J_1(\Delta\phi)\cos[(\omega_o + \omega_\mu)t + \phi_o] \\ + J_1(\Delta\phi)\cos[(\omega_o - \omega_\mu)t + \phi_o] \\ + \ldots\ldots \end{aligned} \tag{5}$$

where ω_o, ω_μ are angular frequencies of the optical and microwave beams and for $\Delta\phi < 1$,

$$J_1(\Delta\phi) \simeq \frac{\Delta\phi}{2} - \frac{\Delta\phi^3}{2^2 2!} + O(\Delta\phi) \tag{6}$$

From Eqs. (4) and (6) we estimate that approximately 5 percent of the optical power will be converted into the sideband, at an applied bias of 20 volts. Assuming a total 3 dB transmission loss through the waveguide, a one watt CO_2 laser will give 50 mW microwave modulated output signal.

2.5 Experimental

Our experiment arrangement is shown in Fig. 1. A stable single frequency TEM_{oo} mode CO_2 laser is injected into a Mach-Zehnder interferometer indicated by the dashed rectangle. M_1 and M_2 are two reflecting mirrors. F denotes the thin film modulator and is mounted on a rotating platform. S represents a 50/50 beam splitter. The IR mixer is a PbSnTe photodiode having a sensitive area ~ 0.0018 cm^2. The laser radiation is split into two beams by a germanium acoustooptic Bragg deflector (Ref. 11). The frequency of the deflected beam is up-shifted by f_a = 25.8 MHz, and is directed toward a folding mirror M_2. The unshifted beam at the molecular resonance f_o is controlled by the mirror M_1, which reflects the beam toward the thin film modulator F. By adjusting the angle of the input coupler with respect to the incident beam a 10.6 μm guided-wave TE mode is excited in the film. The phase-shifted beam is coupled out of the film by the output grating coupler and is recombined with the up-shifted $f_o + f_a$ beam by a beam splitter S. The phase-shifted rf signal generated by the IR mixer is amplified through a narrow-band tuned amplifier and fed into the vector voltmeter (HP8405A). The reference channel of the vector voltmeter is nulled with a properly attenuated signal from the VHF oscillator (HP3200B) used to drive the Bragg cell.

FIG. 1

SCHEMATIC DIAGRAM OF THE EXPERIMENTAL SETUP – FOR THE PHASE SHIFT MEASUREMENTS

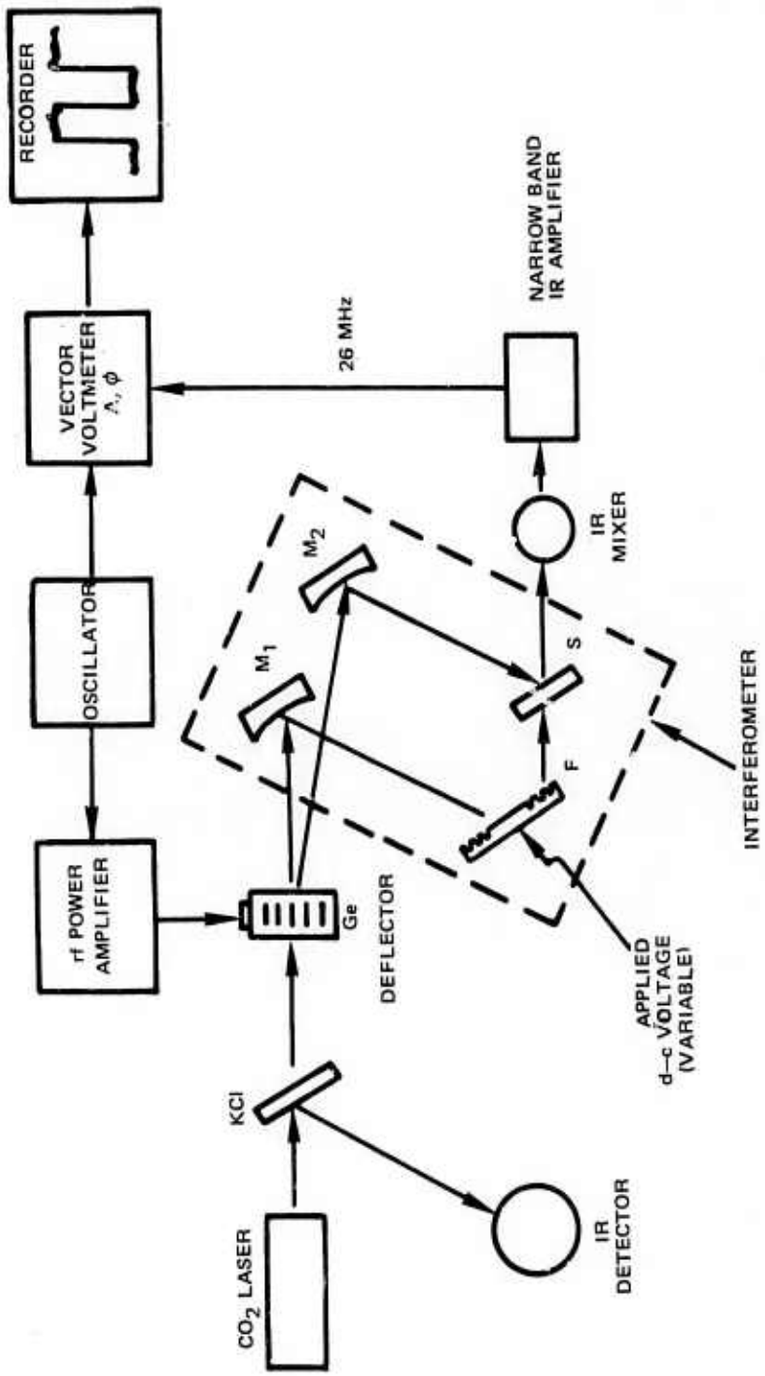

The phase angle $\Delta\phi$ as a function of the reverse-bias voltage on the Schottky barrier electrode can be obtained directly from the front panel of the vector voltmeter or from its recording channel chart. The results are shown in Fig. 2 for two GaAs thin film modulators used in our studies. The first sample, 1EP 658A, has an electrode length of 0.5 cm, and a film thickness of $\sim$ 26 μm. The second sample, 1EP 738A, has an electrode length of 1.0 cm and a film thickness of 17.3 μm. The solid curves represent the calculated $\Delta\phi$ values for the two samples using an r_{41} value of 1.2×10^{-10} cm/V. The maximum long term drift in phase angle is approximately $\pm 2.0^{\circ}$. To demonstrate our system reproducibility, we plotted in Fig. 2 the measured $\Delta\phi$ values versus V obtained from three consecutive runs, which were preformed over a time period of several minutes without replacing the two beams at zero bias. The measured $\Delta\phi$ values are in good agreement with the calculated values to well within the accuracy of measurement. The linearity of this $\Delta\phi$ versus V plot over a large range of V values indicates that our thin films have a depletion depth as large as the film thickness at or near zero bias and are relatively free from residual birefringence due to strain or nonuniformity. Good quality, high resistivity GaAs epilayers are now available in very large size (area > 1 in^2).

2.6 Conclusion

In conclusion, high resistivity GaAs thin films chemically deposited on n^+ GaAs substrates by vapor epitaxy have proved to be good phase modulators for the 10.6 μm CO_2 laser. Our results show that a significant decrease in the half-wave voltage V_π by at least two orders of magnitude can be obtained by using high resistivity thin film modulators. For thin films having relatively high free carrier concentration ($N_f \gtrsim 2 \times 10^{14}$ cm^{-3}), our results indicated that no significant phase shift can be measured until the reverse-bias voltage exceeds at least 20 volts, consistent with our calculated values for a 20 μm depletion depth in thin films of $N_f \simeq 2 \times 10^{14}$ cm^{-3}. Furthermore, our trade-off analysis, based on present technological development, indicates that, among all known methods of electrooptic modulation, high resistivity thin film waveguides are the most promising and practical devices to produce ultra-wideband (> 1 GHz) modulated or chirped signals at the 10.6 μm CO_2 laser wavelength.

FIG. 2

THE MEASURED PHASE–SHIFT OF TE_0 GUIDED–WAVE MODE IN TWO GaAs THIN FILM AS A FUNCTION OF REVERSE–BIAS VOLTAGE.

THE SAMPLE 1EP 658A HAS AN ACTIVE LENGTH 0,5 cm AND A THICKNESS OF 26 μm;
THE SAMPLE 1EP 738A HAS AN ACTIVE LENGTH 1,0 cm AND A THICKNESS OF 17,3 μm.

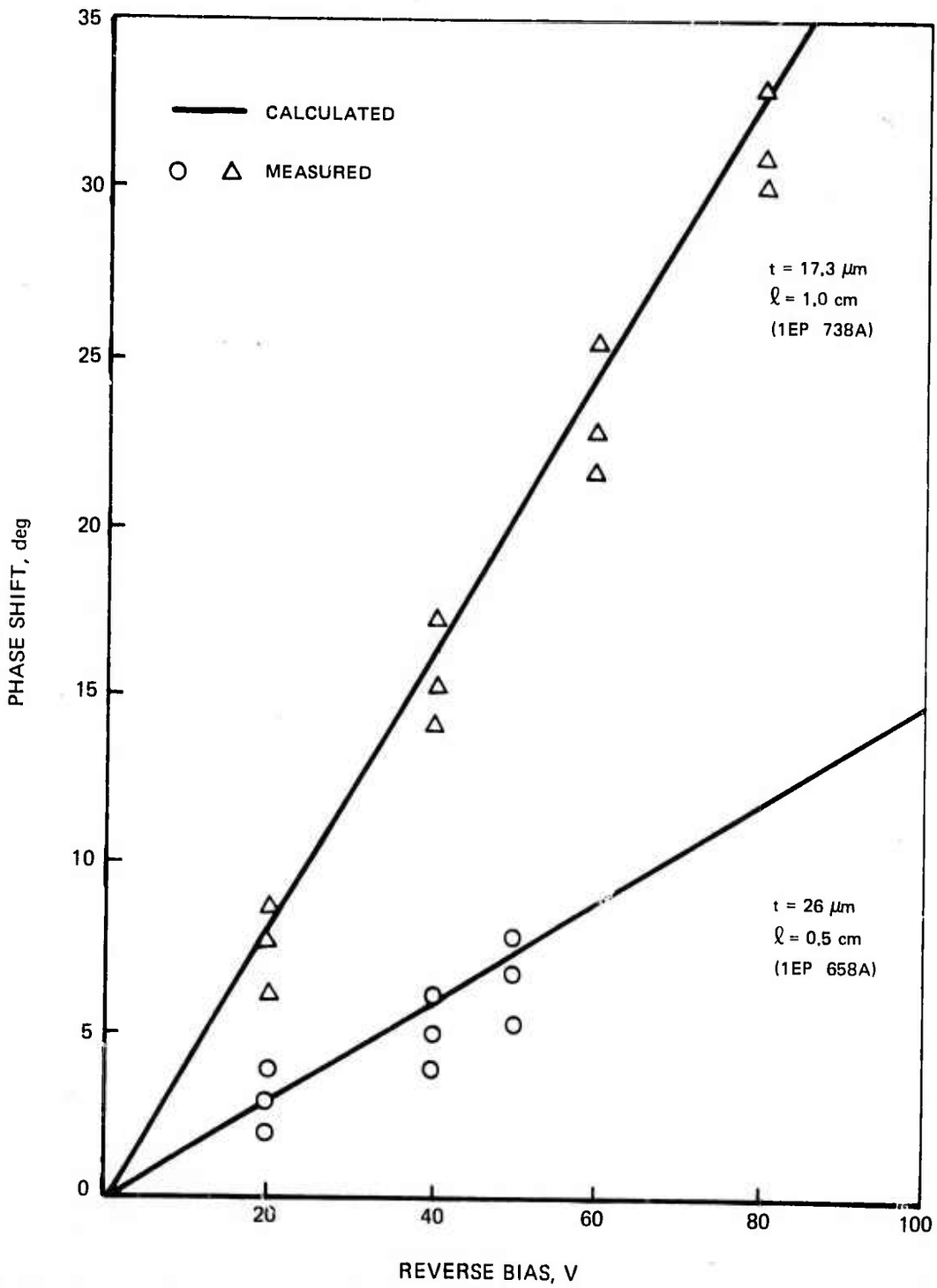

3.0 OPTICAL WAVEGUIDE STRUCTURES

3.1 Introduction

Thin film optical waveguides suitable for phase-modulating a 10.6 μm guided-wave at microwave frequencies must conform to the following basic specifications:

1) Large area films of (100) orientation; the longer the interaction length the greater the phase shift. Dimensions of 4 cm x 1 cm along <110> directions are adequate for our purpose. This allows 3 cm for the interaction length and 0.5 cm for each grating coupler.

2) Correct thickness and good thickness uniformity; for optimum wavelength and modulation the layer thickness must be on the order of 10 μm and must be uniform to within 10%.

3) The supporting substrate; to reduce microwave transmission loss, the conductivity of the substrate must be close to that of a metal. On the other hand, optical transmission loss at the film and metal interface can be significant especially for thin film layer thickness less than 20 μm.

4) Low free carrier concentration (high resistivity); to assure low optical absorption losses, a high frequency of electrical response, and large depletion width (> 30 μm) at zero bias, the carrier concentration in the thin film layer must not be more than $10^{12}/cm^3$.

5) Good surface smoothness and flatness; to allow highly accurate phase gratings to be produced and to assure low scattering losses, the free surface of the film must be smooth to within 0.3 μm over the entire interaction length, and flat to within 1.0 μm in the region of the gratings.

6) Good smoothness and flatness, and sharp definition of the thin film interface; the smoothness and flatness requirements are the same as in 5 above. The sharpness of the interface between heavily doped substrate and the highly pure (or high resistivity) epi layer must be such that the carrier concentration will decrease from substrate values to $10^{15}/cm^3$ or less within 0.2 μm, and from thence to $10^{12}/cm^3$ or less within 0.8 μm.

7) Optical waveguide configuration must be designed to provide the best interface with the microwave ridge-waveguide structure.

Clearly from specification #3, the usual GaAs n/n^+ epitaxial thin film waveguide structure, which has been extensively investigated in the past (Refs. 1 to 6), is not the best choice for the present program application. A large effort has been made during this interim period to determine an optimum thin film modulator configuration

to afford the maximum probability of success. As one initial step, a three pronged approach has been followed. Figure 3 indicates the configurations of the three different approaches. Two of these three approaches, Fig. 3(b) and (c) utilize epitaxial growth techniques to deposit layers with good waveguide properties. The other depends upon chemo-mechanical and chemical thinning of bulk GaAs wafers to waveguide dimensions. In all three approaches, we must provide waveguiding material to meet the above specifications. In the case of epitaxial thin films, the epi-substrate interface must be sharply defined. In other words, a transition from n^+ substrate to the waveguiding layer must be made within one micrometer. Ideally we would like to make the transition from $10^{12}/cm^3$ levels to $10^{15}/cm^3$ levels in 0.8 μm and from $10^{15}/cm^3$ to substrate doping levels (usually $10^{18}/cm^3$) in 0.2 μm. Also to reduce microwave losses, the n^+ substrate must be thinned to less than 5 μm, in the 1 mm wide interaction region. This can be accomplished by an etch-stop technique.

In the following we shall discuss each approach in greater detail. At the present stage of development, the first approach chemo-mechanical thinning of bulk GaAs wafers is progressing far ahead of the other two. Therefore, it is most likely the configuration that will fulfill the present program goal. Technical discussions will also be given in this report on the other two approaches.

3.2 Fabrication and Processing Techniques

3.2.1 Chemo-Mechanical Thinning Technique

Thin films can be made by careful polishing of bulk wafers. This is a very painstaking and time consuming operation but many wafers can be processed at one time. In fact it is necessary to polish three or more wafers simultaneously on each mounting disk to get good results. It is also absolutely essential that the starting bulk wafer have smooth, flat, strain-free reference surfaces. Typically, starting thickness is about 0.025". The initial thinning involves removal of .005" to .007" of material with respect to the reference surface. The final polishing of the reference surface is done by the chemo-mechanical technique, in which the mechanical action is one of friction only between wafer surface and pad surface. The wafers are next demounted and thoroughly cleaned before proceeding with the rest of the thinning operations. The wafers are then remounted with a special low-viscosity wax using sufficient weight uniformly distributed over the wafer surface to assure a thin uniform film of wax between wafer and polishing block. When the wax has hardened the weights are removed and the excess wax is stripped away by solvent rinses. Final thinning to waveguide dimensions is achieved by a combination of mechanical, chemo-mechanical and chemical procedures. The thickness of the GaAs wafer is monitored and polishing is stopped when the desired dimensions are achieved.

It is necessary to fabricate grating structures on bulk wafers since the grating fabrication steps are difficult to perform once the wafer has been thinned to waveguide dimensions.

FIG. 3

THREE POSSIBLE THIN FILM WAVEGUIDE CONFIGURATIONS

a) THINNING OF BULK WAFERS

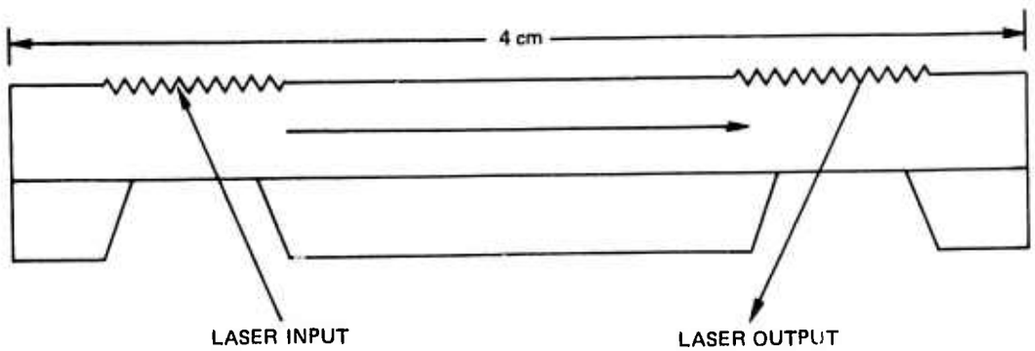

b) EPITAXIAL WAFER WITH BURIED GRATING CORRUGATIONS

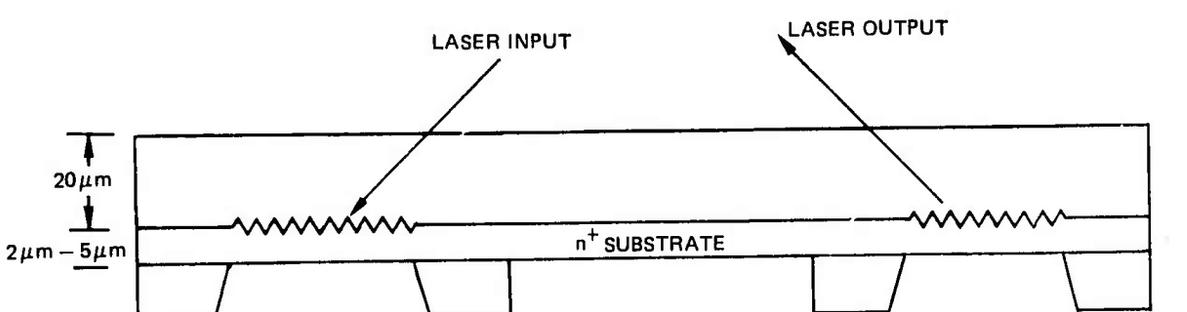

c) EPITAXIAL WAFER WITH SURFACE GRATING CORRUGATIONS

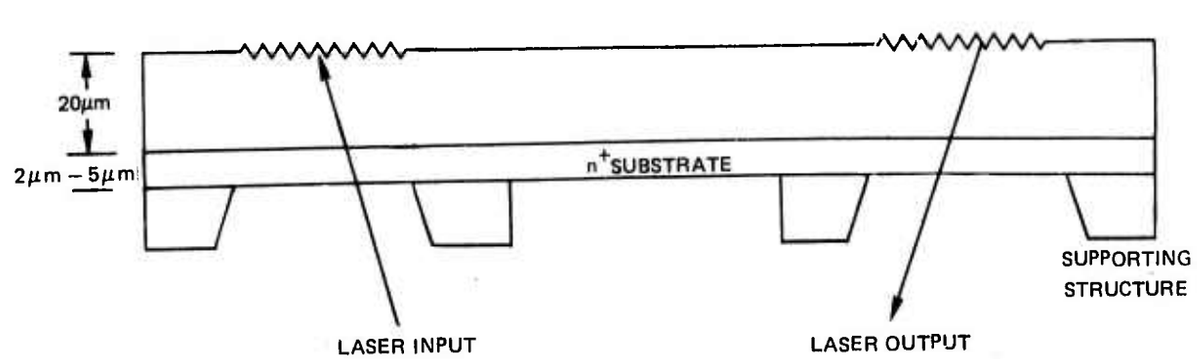

To evaluate the quality of optical waveguide structures obtained by this technique three test wafers were prepared in our initial attempt. The range of measured thickness and thickness uniformity is listed in Table II. A portion of one of the IR fringe recordings is shown in Fig. 4. Unlike spectra of epi wafers, these spectra show very strong fringes at wavelengths as short as 3.0 μm. This is because the fringes are set up by multiple reflections between two semiconductor-air interfaces instead of between one semiconductor-air interface and one semiconductor-semiconductor interface. Narrow strips cleaved from these Cr-doped GaAs thin films were used for the microwave transmission measurements, as described in Section 4.0. It is noteworthy that very thin GaAs wafers are quite flexible and all of the test wafers bent under their own weight when picked up near the edge.

The next batch of thinned wafers was processed while still on the polishing block. This batch was used to establish a metal plating technique intended to both support the thin films and provide good heat sinking for high power applications. To improve waveguiding properties, a buffer layer of 2.5 μm of ZnS was sputtered onto the GaAs using an rf apparatus. This was done one wafer at a time, and at a controlled sputtering rate in order to reduce mechanical stresses which may be developed in these thin films. Two approaches were used to produce a metal supporting structure; the first method involves rf sputtering a thick metal layer on the GaAs wafer, the other involves an electrolytic plating technique. Both approaches have yielded encouraging results. In the first case, the thick metal deposition by rf sputtering actually involves three steps. The first deposition is chromium, to provide good adhesion between the ZnS buffer layer and the subsequent metal. The second layer is gold, to prevent formation of an oxide film between the chromium and the thick metal. The thick metal itself is the third layer. Figure 5 shows three substrates with 32 μm of copper rf sputtered on the grating side of the GaAs. The metal surface is used as the reference for chemo-mechanical thinning of the GaAs from its original thickness down to 20-25 μm.

To deposit a thick layer of gold on a GaAs surface by electrolytic plating process, a very thin rf sputtered layer of Cr-Au is needed to form a base. After forming this base layer, the entire exposed surface of the mounting block is painted with a high temperature lacquer to prevent its exposure to the plating solution (plating temperature was controlled at 160°F to 170°F). Enough time is allowed for these metallic films to plate to the desired thickness, typically .001" to .0015". A close up view of one of the GaAs thin film waveguides having a .0015" thick gold supporting layer after removal from the polishing block is shown in Fig. 6. This thin film waveguide has been cleaved into two sections. Notice that the Au supporting layer is actually holding the cleaved thin film together. Notice also that warping of the GaAs is evident in Fig. 6. Judging from the contour of this warping we conclude that differential thermal contraction in cooling from plating temperature to room temperature is responsible.

TABLE II

Thickness Measurements of Chemo-Mechanically Thinned GaAs Optical Waveguide

Wafer	Thickness Variation (μm)	
	Min	Max
#1	28.9	34.4
#2	36.4	42.1
#3	33.9	38.2
A	22.0	28.0
B	19.2	26.0
C	17.0	18.5

INTERFERENCE FRINGE SPECTRUM OF GaAs THIN FILM PREPARED BY CHEMO–MECHANICAL TECHNIQUES

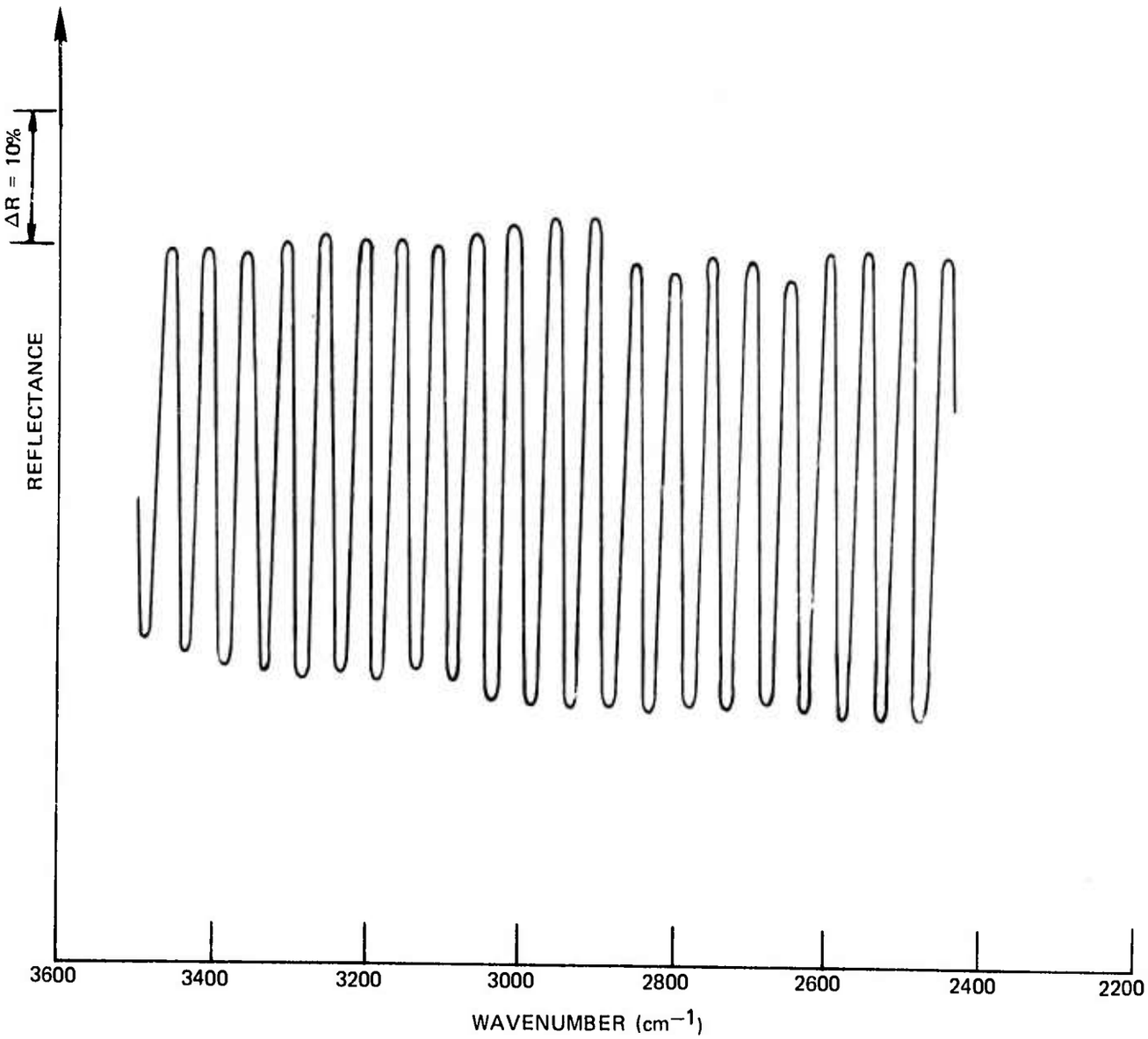

FIG. 5

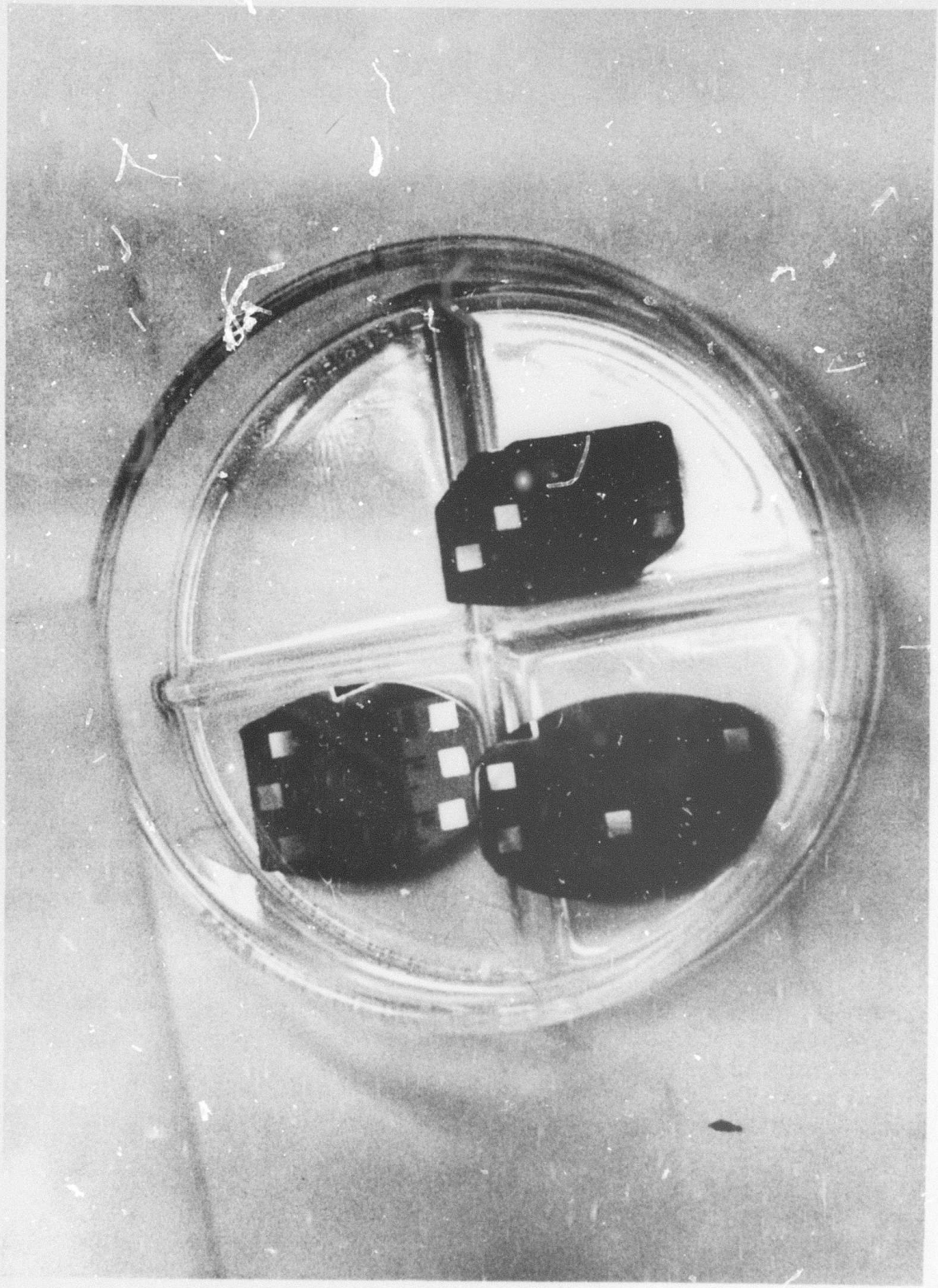

GaAs WAFERS WITH 32 μm (RF SPUTTERED) Cu LAYER

FIG. 6

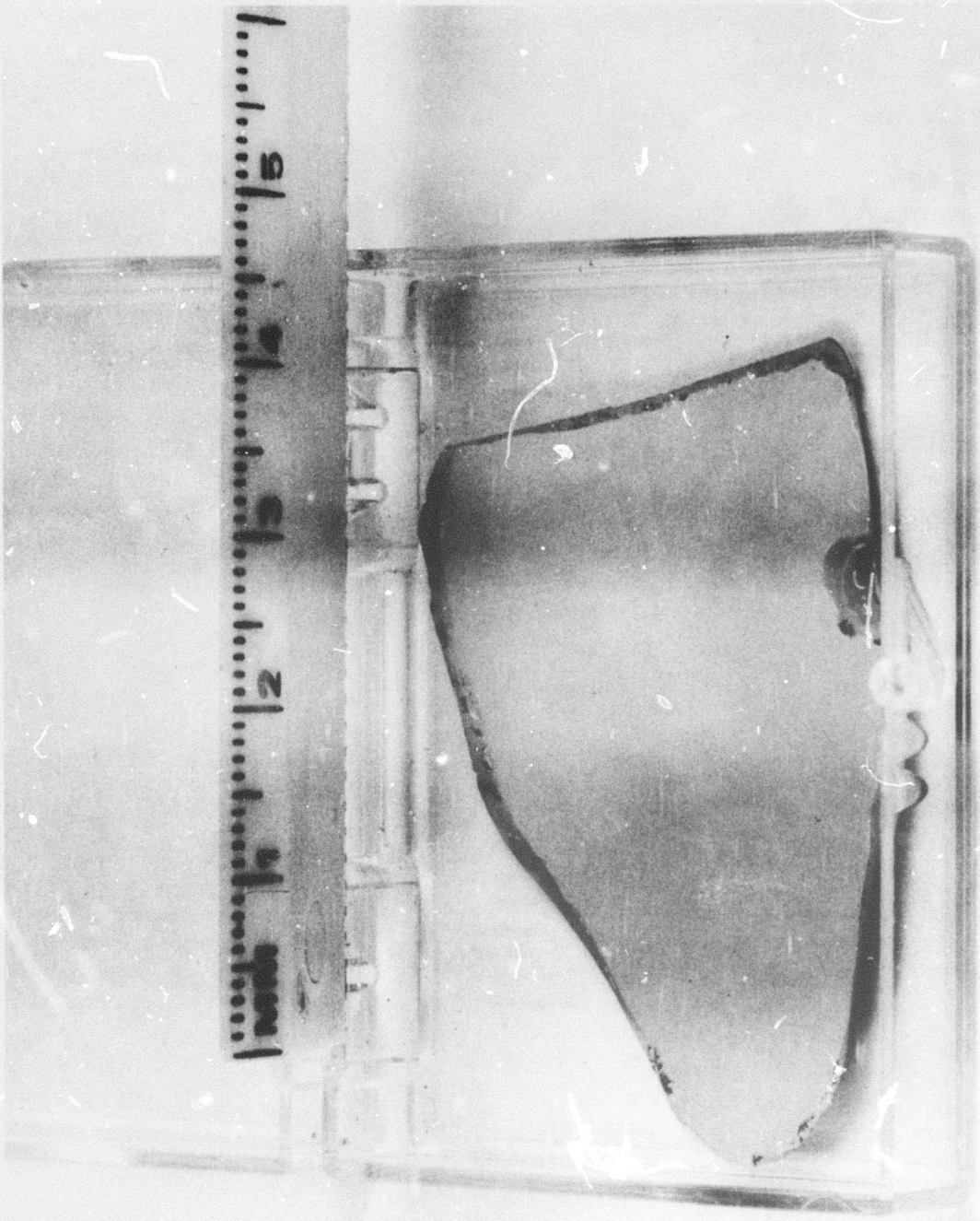

CHEMO–MECHANICALLY POLISHED GaAs THIN FILM HAVING A Au SUPPORTING LAYER OBTAINED BY ELECTRO–PLATING TECHNIQUE

3.2.2 Epitaxial Approach

3.2.2.1 Controlled Growth

All of our epitaixal thin films have been produced in a vapor phase reactor utilizing the $AsCl_3$-Ga transport system with pure (Pd-diffused) H_2 as the carrier gas. The first of the two epitaxial approaches that was pursued involved the buried grating structure. However before such structures were attempted, it was necessary to produce wafer properties basic to good waveguiding. Perhaps the most difficult of the requirements was the creation of epitaxial layers with a very abrupt substrate interface and with very low carrier concentration. Previously we had seen layers with 4 μm to 5 μm thick transition region spanning the mid $10^{13}/cm^3$ to mid $10^{16}/cm^3$ range of carrier concentration. By incorporating Cr doping in our vapor system we have been able to regularly produce epitaxial layers with net carrier concentration below $10^{13}/cm^3$. The chromium is introduced via a bubbler built into the doping-gas supply stream using chromyl chloride (CrO_2Cl_2), a volatile liquid at normal temperature and pressure, as the source of chromium. It was found best to introduce the CrO_2Cl_2 vapor by diffusion into the doping-gas stream rather than by bubbling the gas through the liquid itself. The high chromyl chloride concentrations that resulted from bubbling caused the epitaxial surface to become severely pitted. Table III is a list of Cr-doped epitaxies comparing Schottky barrier (SB) measurements with Hall effect measurements.

Generally, the transition region in these wafers was less than 3 μm thick and in two instances it was not more than one micrometer. The shape and sharpness of the charge carrier profile in the transition region is carefully controlled, especially during its initial epitaxial growth. We have observed that slight changes in our procedure or in our timing strongly affect the interface quality. Figure 7 is a typical Schottky barrier measurement of an epitaxial thin film, VP158, showing the shape and sharpness of the free carrier profile in the interface region. Figure 8 shows a set of interference fringe spectra taken at the cardinal points of a wafer (VP156). The strong fringe structure at 10.6 μm is consistent with a sharply defined epi-substrate interface and smooth epitaxial surfaces.

The next task was to produce large epitaxial wafers with acceptible thickness uniformity. The large size of our reactor tube (35 mm useful bore) and the long constant temperature zone were important factors in determining the thickness uniformity. After several trial runs, the optimum wafer position was pinned down and we were able to produce wafers 5 cm long x 3 cm wide with thickness uniformity of 10% to 20%. A portion of one of these wafers is shown in Fig. 9.

3.2.2.2 Epitaxial Thin Film Growth on Corrugated Substrate

Once we were able to produce epi layers with the required properties for waveguiding, we then proceeded with a novel experiment by attempting the growth of an

TABLE III

Electrical Characteristics of Cr-Doped GaAs Epitaxial Thin Films

	n (cm^{-3})	
Run #	Hall Effect*	Schottky Barrier
148	---	$< 10^{12}$
149	1.4×10^{12}	$< 10^{14}$
150	1.8×10^{12}	---
151	---	$< 10^{13}$
152	1.2×10^{12}	$< 10^{13}$
153	$.7 \times 10^{12}$	$< 10^{13}$
154	1.7×10^{12}	$< 10^{13}$
156	---	$< 10^{13}$
158		$< 10^{13}$
160		$< 10^{13}$

*These numbers must be regarded as upper limits, since the resistance of the epitaxial layer is high enough so that the Cr-doped semi-insulating substrate can no longer be taken as completely effective in electronically isolating the epitaxial layer.

M921513–4

FIG. 7

TYPICAL SCHOTTKY BARRIER MEASUREMENTS TO SHOW THE FREE CARRIER PROFILE

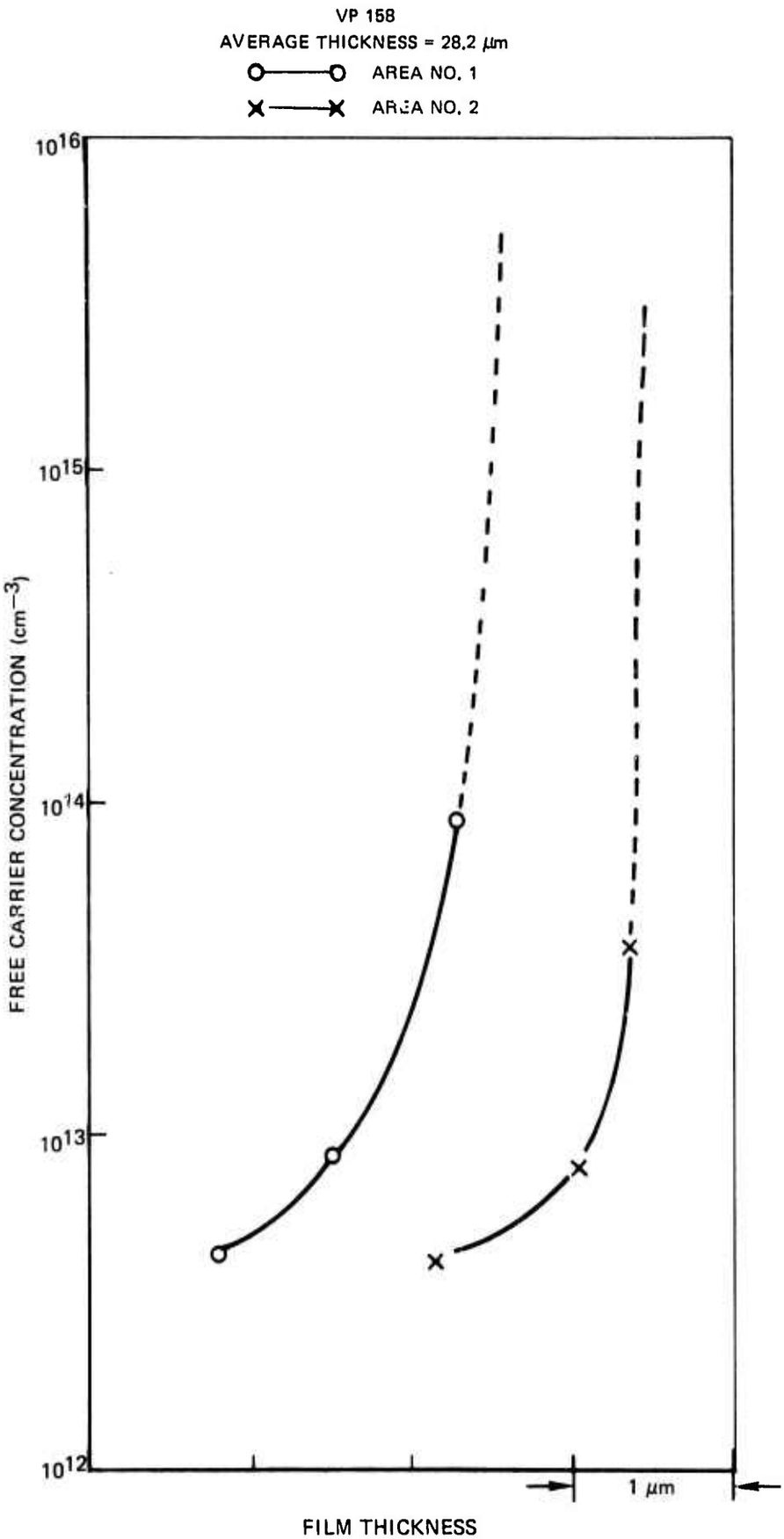

INTERFERENCE FRINGE SPECTRA TAKEN AT THE CARDINAL POINTS OF WAFER VP156

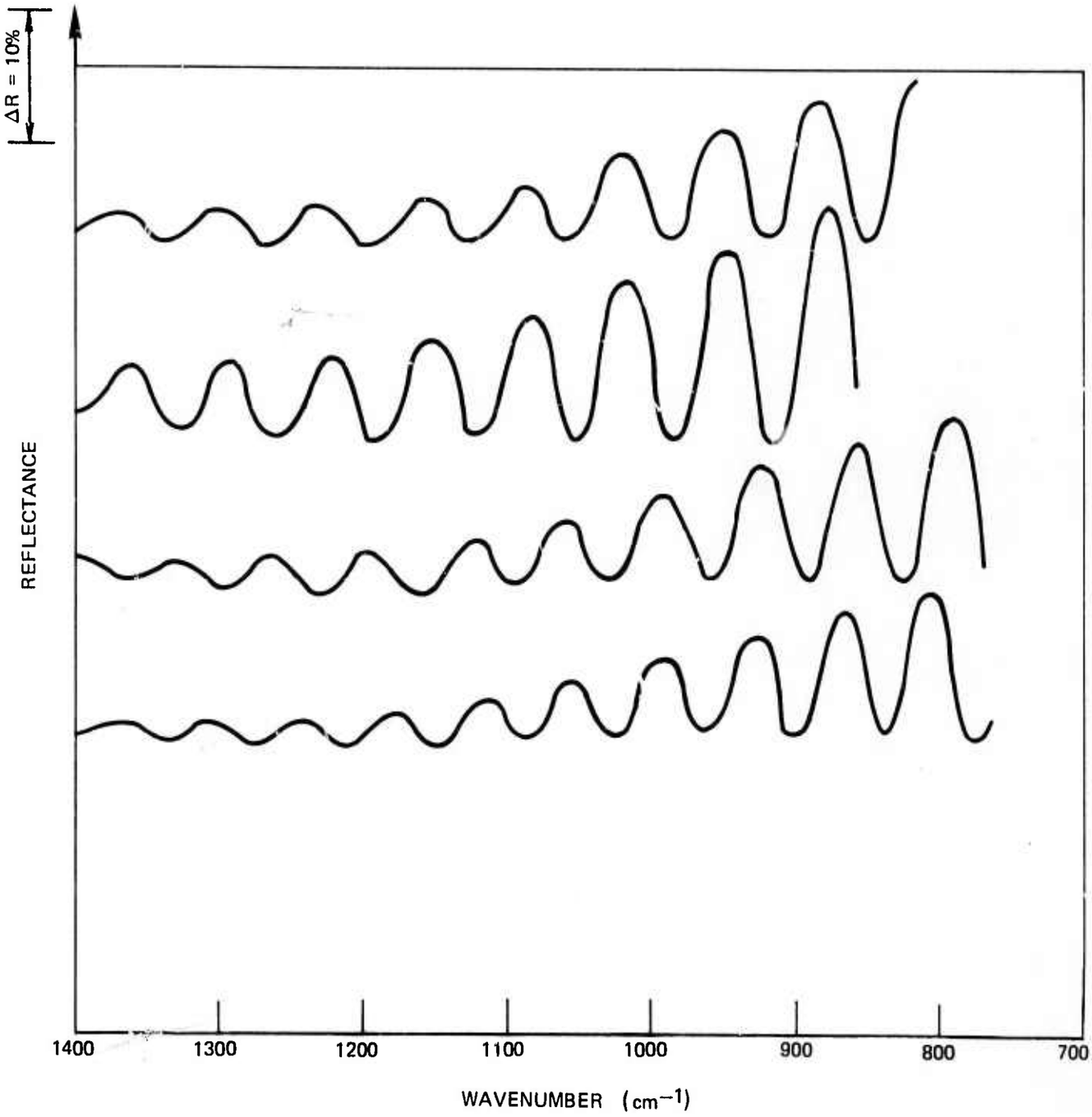

A SECTION OF A LARGE EPITAXIAL WAFER HAVING A 20 μm Cr–DOPED LAYER

M921513–4

FIG. 9

epitaxial thin film on a corrugated n^+ GaAs substrate. The first attempt was directed at producing "buried gratings", using a wafer containing gratings with a 3.5 μm periodicity, 1.5 μm depth, and 1:1 aspect ratio of groove width to ridge width. This attempt was initially considered as the quickest way to obtain data concerning the backward optical coupling scheme. Figures 10 and 11 show photomicrographs at two different magnifications of cleaved and etched sections, taken from a grating wafer after a 12.5 μm thick epitaxial layer had been grown on it. The grating structure has been well preserved and is clearly distinguished at 500X as shown in Fig. 10. Notice that there is no trace of the ridge and groove structure at the epitaxial surface In order to bring out the interface regions for detailed examination a light etch is necessary. The formulation used for this purpose is a water solution of KOH + $K_3Fe(CN)_6$ in the weight ratio 10:2:2, sometimes called "Murakami stain". The cleaved surfaces of all samples were swab-etched for 5 seconds and thoroughly rinsed in running H_2O before microscope examinations. The "cap" that appears to be present on the ridges, as shown in Fig. 10, is revealed in greater detail in the SEM photomicrograph of Fig. 11. This cap is actually seen to be a ramp-like etch structure that marks the transition from substrate to epitaxial layer. In an ideal structure this would appear more like a step than a ramp, in keeping with the abrupt electrical and optical character of the junction desired for good waveguiding. It appears from Fig. 11 that the thickness of the interface region in this wafer is about 1.5 μm.

Our next attempt was to produce epi-layers on corrugated substrates having smaller periods in the range from 2.5 to 2.8 μm. Figures 12 and 13 show cleaved sections of wafers with such buried gratings. Notice that these gratings are markedly different than before; the ridges are sharper and the grooves are much wider than the ridges. A closer examination reveals that there exists structural (or doping) faults in several locations within the grating area. The size and distribution of these faults suggest that they could have a deleterious effect on grating efficiency, thus their cause and subsequent removal merit some attention. These imperfections were thought to be due to crystal damage introduced during the grating fabrication. To ascertain that the greater part of the epitaxial layer above the buried grating was of good crystal quality, Laue back diffraction photograms were taken in one sample. The results shown in Fig. 14 reveal a diffraction pattern with sharp spots indicative of high crystal perfection.

3.2.2.3 Etch-Stop System

As pointed out in Section 3.2.1 the usual n/n^+ GaAs epitaxial thin films are not compatible with the modulation scheme intended for this program. To meet all the specifications, one alternative is to modify the n/n^+ structure by removing the n^+ substrate material. In this case, not less than 2 μm nor more than 5 μm of substrate must remain for optimum performance of the finished device. This thinning of the substrate may be done over the entire wafer or, if a more rugged structure is desired, only in the active regions of the wafer. The application of standard mate-

M921513–4

FIG. 10

CLEANED AND ETCHED SECTION SHOWING
BURIED GRATING OF 3.5 μm PERIODICITY

OPTICAL MICROGRAPH, OBLIQUE ILLUMINATION

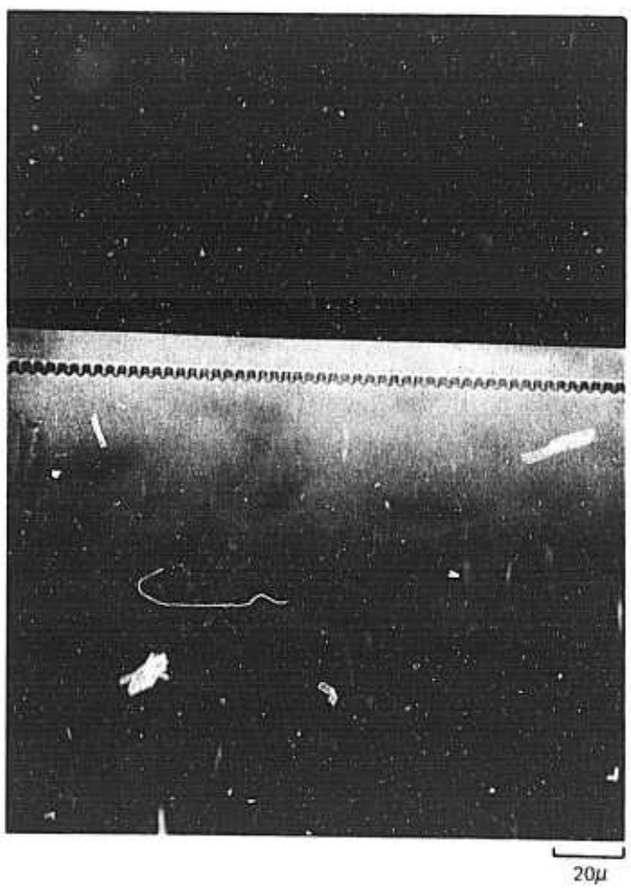

M921513–4

FIG. 11

SEM MICROGRAPH AT OBLIQUE ANGLE
SHOWING RAMP–LIKE ETCH STRUCTURE
AT SUBSTRATE–EPI INTERFACE

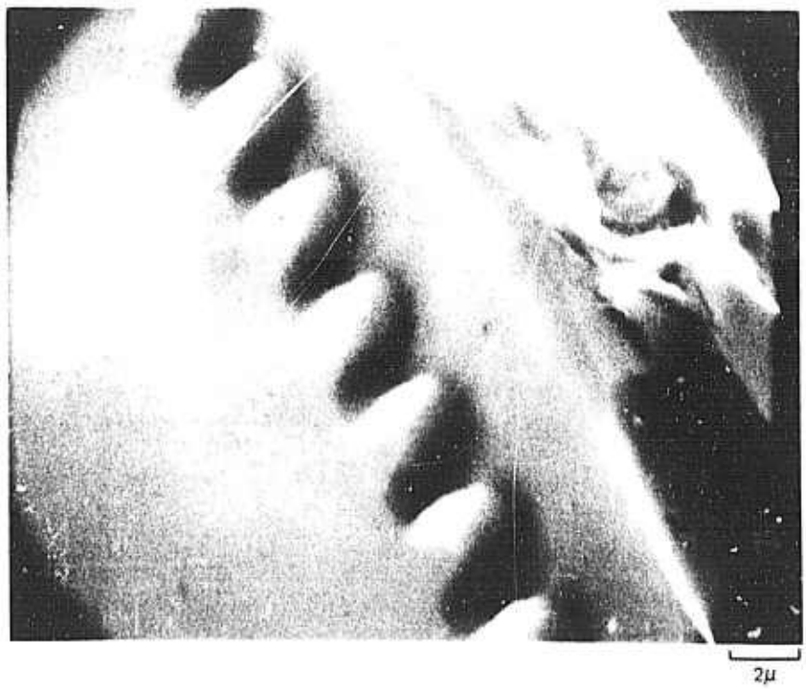

M921513–4

FIG. 12

SEM MICROGRAPH OF 2.71 μm GRATING

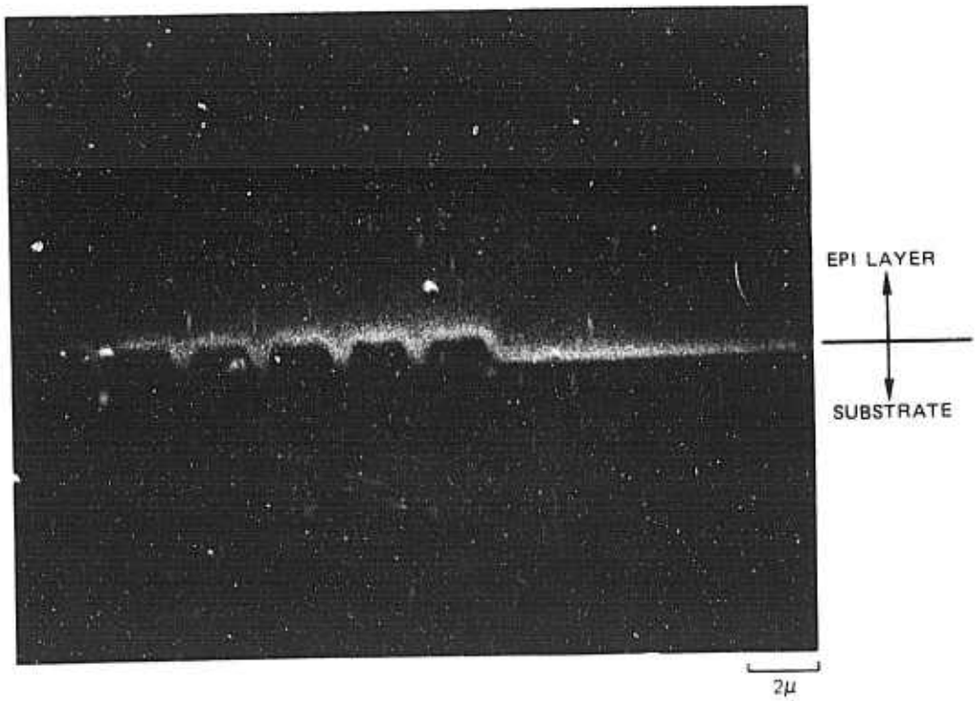

FIG. 13

SEM MICROGRAPH OF 2.71 μm GRATING

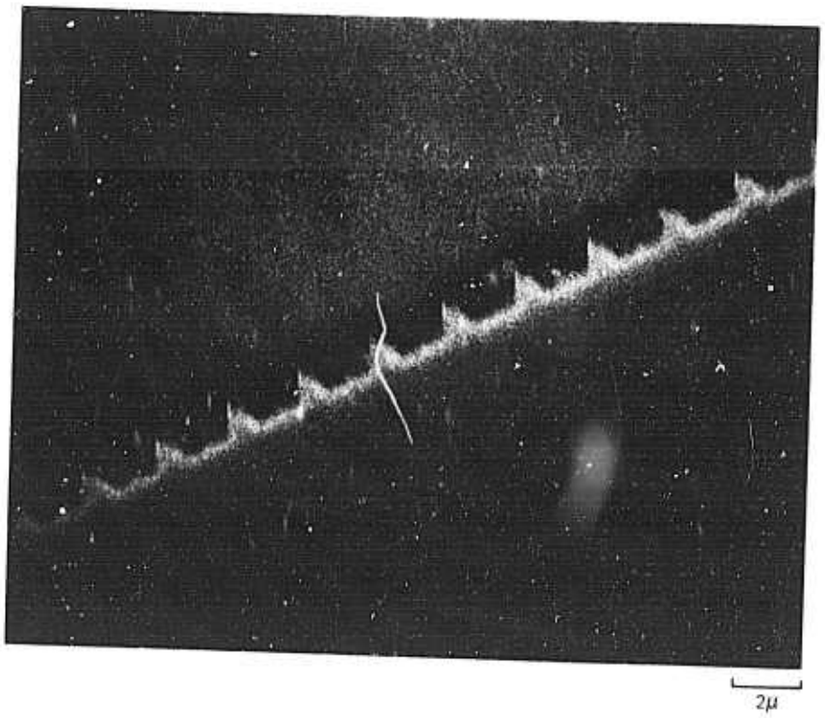

FIG. 14

LAUE BACK–DIFFRACTION PATTERN OF GaAs THIN FILM
EPITAXIALLY GROWN ON A CORRUGATED SUBSTRATE

rial removal techniques to produce such structures requires a high degree of precision in process control and in measurement and is time consuming. In the following a description of these methods and their results is presented. A good technique which we refer to as the chemical etch-stop technique, is based on a self-controlling materials removal action. Presently we are experimenting with such an etch-stop system. An etch-stop system depends on its ability to produce rapid interaction between the dissolving semiconductor and the etchant solution to form an insoluble barrier on the semiconductor that protects it against further dissolution. For example, in GaAs, a thin p-type layer made by heavy cadmium doping will stop the etching action of a solution containing an appreciable concentration of hydroxyl ions by forming a thin adherent film of insoluble $Cd(OH)_2$. The solubility of etchant products can be described by the solubility product contant (K_{sp}) defined as $[C]\,[A] = K_{sp}$ where [C] indicates the cation, or metal ion concentration (in moles/liter) and [A] indicates the anion or non-metal ion concentration. A simple calculation shows that the solubility product constant (K_{sp}) need only be 10^{-7} or so to form a precipitate after dissolution of as little as 0.05 mg of $10^{18}/cm^3$ doped material in 100 ml of etchant. Thus for GaAs, etching action would cease after dissolving a 0.2 μm thick layer doped with $10^{18}/cm^3$ of cadmium. For our purposes however an n-type etch stop is preferred. Sulfur is an n-type dopant in GaAs and it promises a wide range of possibilities because of the very low solubility of many sulfides and sulfates. Seven chemical systems were identified involving sulfur-doped material. To properly evaluate these systems we re-acquired a supply of test wafers. The preparation of GaAs epitaxies heavily doped with sulfur was undertaken via vapor phase growth in a system separate from that used for Cr-doping. Several wafers with epitaxial layers 4 μm to 5 μm thick were grown with sulfur doping ranging from $5 \times 10^{17}/cm^3$ to $9 \times 10^{18}/cm^3$, however poor control was experienced. Subsequently the diffuser element in the Pd-H_2 purifier supplying this system failed. Further experiments will be resumed as soon as this unit is put back in service.

3.3 Optical Coupling by Backward Diffraction

3.3.1 Theory

Optical coupling from a thin film waveguide by using etched gratings has been numerically analyzed (Ref. 6) by Chang and coworkers. Results indicate that the highest coupling efficiency can be achieved when the grating periodicity is chosen for first order diffraction by backward excitation from the substrate. It turns out that when guided-wave mode is excited in the backward direction, as shown in Fig. 3, power loss diffracted to various orders as well as to modes other than the guided-wave modes can be eliminated. This is not true for forward excitation from air or from the substrate. This may be better understood by examining the allowed range of β, the propagating constant for various waveguide modes. Generally, excitation of a guided-wave mode is established if phase matching conditions are satisfied:

$$\beta_m = k\sin\theta + \frac{2\pi}{L} N \qquad \text{(from air)} \qquad (7)$$

$$\beta_m = n_o k \sin\theta + \frac{2\pi}{L} N \qquad \text{(from substrate)} \qquad (8)$$

Where L is grating periodicity, N is the diffraction order, θ is the angle of incidence measured from the normal, k is the propagation constant in free space.

We have previously (Ref. 1) computed the β_m values for TE and TM modes in a GaAs n/n^+ waveguide structure, using the analysis of Tien and Ulrich (Ref. 12). The waveguide configurations required for this program differ somewhat from the n/n^+ structure. For a single layer structure such as shown in Fig. 3(a), the indices n_o, n_1 and n_2 are 1.0, 3.275 and 1.0, respectively. The general formulations for semi-infinite planar waveguides having a thickness d that can support a number of TE and TM modes are given by (Ref. 12)

$$d = \begin{cases} (1/b_1)[m\pi + \tan^{-1}(\rho_o/b_1) + \tan^{-1}(\rho_2/b_1)] & \text{(TE)} \quad (9) \\ (1/b_1)\left[m\pi + \tan^{-1}\left(\dfrac{n_1^2\rho_o}{n_o^2 b_1}\right) + \tan^{-1}\left(\dfrac{n_1^2\rho_2}{n_2^2 b_1}\right)\right] & \text{(TM)} \quad (10) \end{cases}$$

where

$$b_1^2 = (kn_1)^2 - \beta^2$$

$$\rho_o^2 = \beta^2 - (kn_o)^2 \qquad (11)$$

$$\rho_2^2 = \beta^2 - (kn_2)^2$$

The indices 0, 1, 2 refer to the substrate, the guiding layer and the superstrate. Results of Eq. (9) are plotted as shown in Fig. 15 for a single layer structure where $n_o = 1.0$, $n_1 = 3.275$ and $n_2 = 1.0$. To increase isolation and discrimination between modes, we also consider the use of a multilayer structure which consists of a GaAs guiding layer sandwiched between two thin layers of CdTe. In this case, the refractive indices are $n_o = 2.6$, $n_1 = 3.275$ and $n_2 = 2.6$. The claculated β/k values for the TE modes of this structure are shown in Fig. 16.

The advantages of these structures are: (1) it is possible to utilize backward excitation to improve the optical coupling efficiency, (2) the optical and microwave propagation losses are greatly reduced, (3) electrodes need not be Schottky barrier junctions and (4) an alternating voltage can be applied to the device without the need of a bias. The major problem in using these structures is their weak structural strength which can easily cause breakage and fracture along the crystal cleavage planes. To overcome this difficulty, efforts were made to develop techniques for

FIG. 15

SINGLE LAYER GaAs THIN FILM WAVEGUIDE STRUCTURE

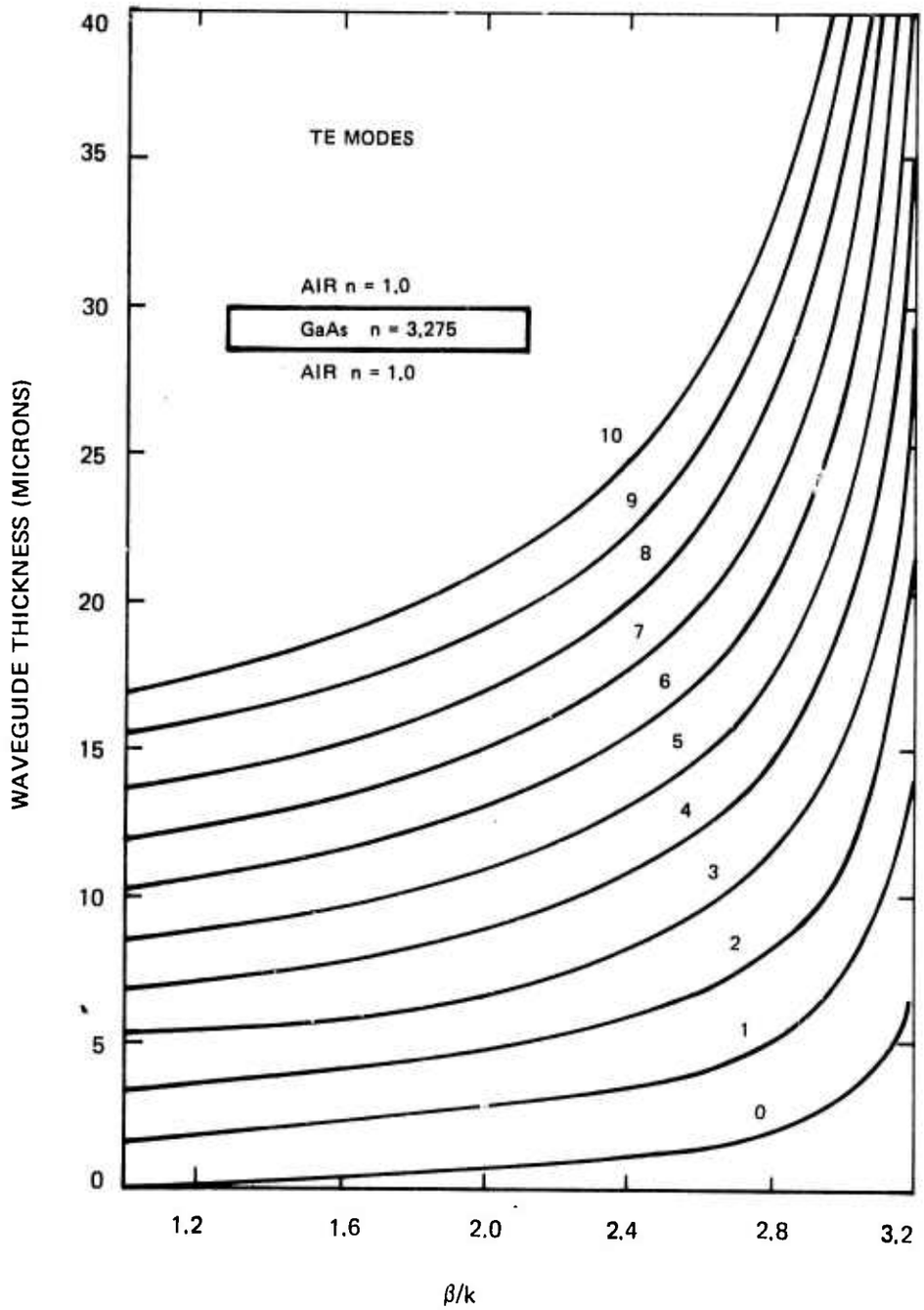

FIG. 16

MULTILAYER ZnS/GaAs/ZnS THIN FILM WAVEGUIDE STRUCTURE

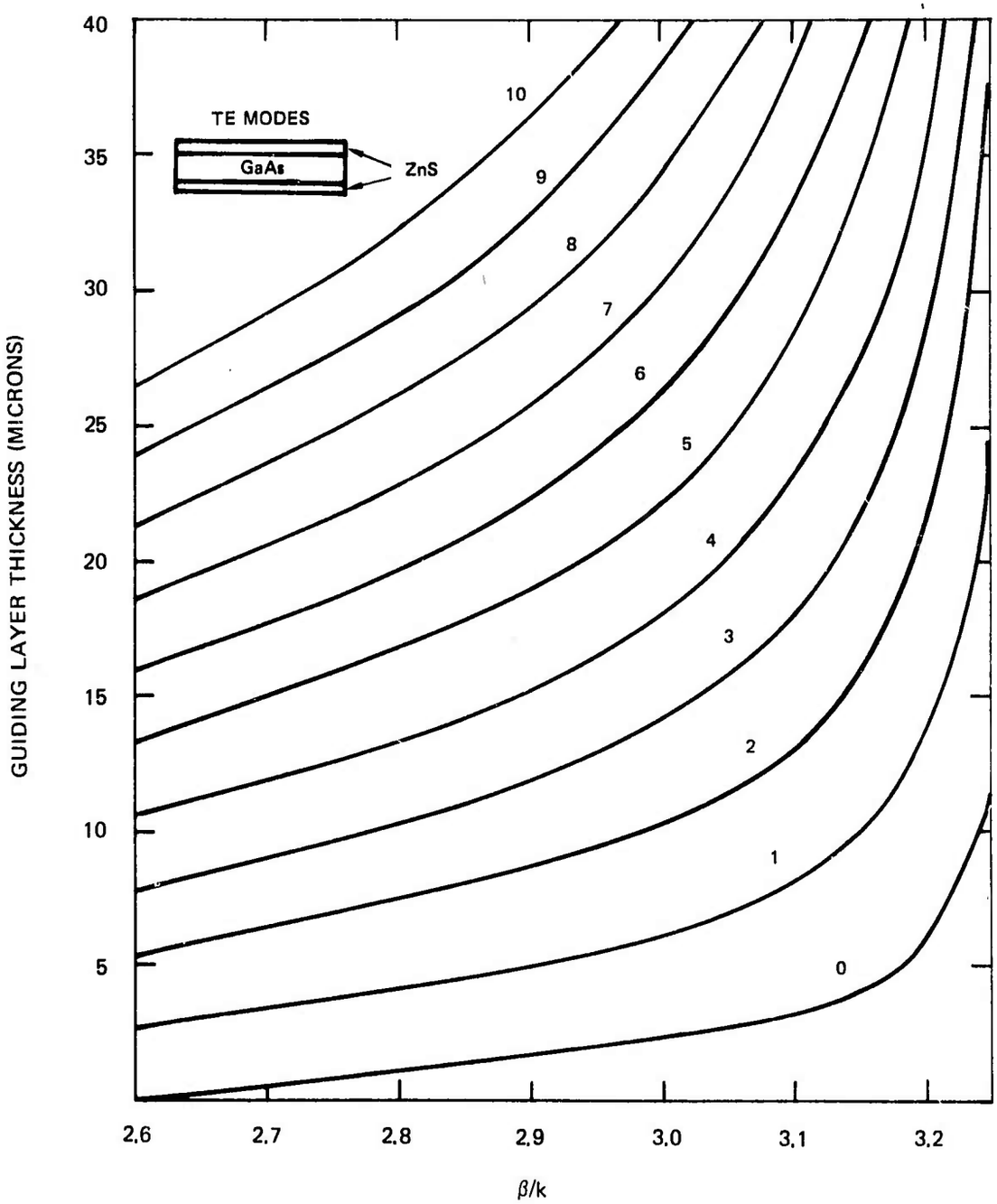

ruggedizing these structures. This was accomplished by depositing a supporting metallic layer, which also serves as one of the electrodes. Details of these procedures have been described in Section 3.2.

There exists three sets of modes for a given optical waveguide. One is a finite set of discrete modes known as guided modes having propagation constants β_m where m = 0, 1, 2, ... The other two are infinite sets of continuous modes consisting of the so-called "air modes" and "substrate modes". In the case of air mode ($0 \leq \beta \leq k$), the field is propagating in both the air and the substrate region. When $k \leq \beta \leq n_o k$, the field is evanescent in the air region and is propagating in the substrate. Figure 17 shows the region where these modes occur and the range of β values allowed by two excitation schemes. Among a number of other possibilities, Fig. 17(b) shows the worst case whereas Fig. 17(c) shows the most efficient excitation scheme. It is obvious from Fig. 17 that in order to achieve the most efficient coupling, the periodicity of grating L must be very small. In the case of GaAs thin film waveguides, Eq. (8) indicates that the values of L must lie within $2.5\ \mu m \leq L \leq 3.2\ \mu m$. Figure 18 is a plot of the calculated angle of coupling θ from the substrate side as a function of the grating period L, for various TE modes in a 20 m thick GaAs thin film waveguide.

The backward coupling efficiency of a phase grating with etched grooves is given by (Ref. 6)

$$\eta = \frac{k^4 |C_s|^2 \Lambda}{8\omega\mu_o b_o} \left(\frac{1 - e^{-\alpha\Lambda}}{\alpha\Lambda} \right)^2 \tag{12}$$

where C_s is the backward scattering coefficient of the sth diffraction order. Λ is the grating area covered by the incident beam and is the product of L and the number of grating line elements and $b_o = n_2 k \cos\theta$. Other symbols have their usual meanings. Notice that the function, $(1 - e^{-x})^2/x^2$ in Eq. (12) has a maximum value for x = 1.25. It should be noted also that η is directly proportional to C_s^2. An examination of the complex expression for C_s given in Ref. 6 indicates that

$$\eta \propto \Delta n^4 \delta^2 / \lambda^4 \tag{13}$$

which means that the coupling efficiency depends strongly on the difference of refractive index Δn between the guiding layer and the superstrate and on the laser wavelength λ. Furthermore η increases with an increasing groove depth δ. Numerical results (Ref. 6) indicate a coupling efficiency of $\gtrsim 50\%$ can be achieved by directing a CO_2 laser beam toward a GaAs guiding layer from the backside, with an etched grating coupler fabricated on the front surface having a $\Delta n = 2.75$. Under a similar condition, $\eta \simeq 70\%$ can be obtained for a Ge waveguide, because in this case, $\Delta n = 3.0$.

FIG. 17

a) VARIOUS MODES OF UNPERTURBED THIN FILM WAVEGUIDE

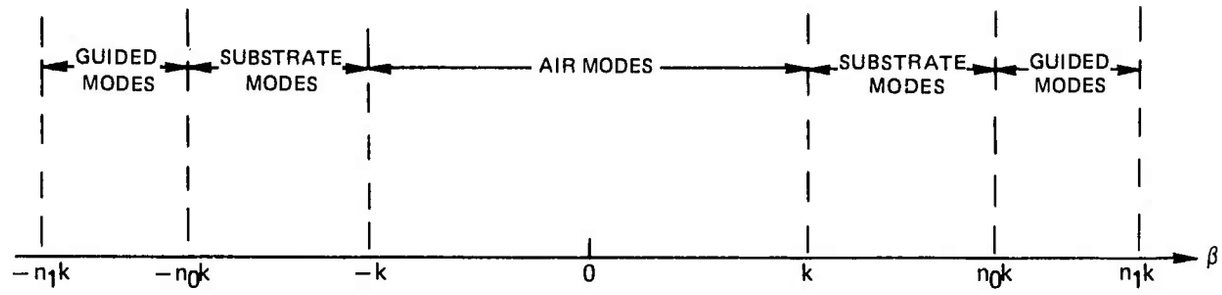

b) POSSIBLE MODES TO BE EXCITED FROM THE AIR SIDE IN THE FORWARD DIRECTION

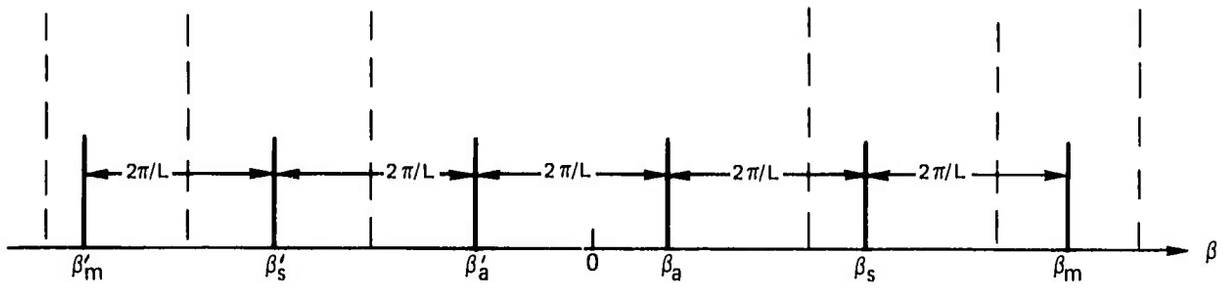

c) POSSIBLE MODES TO BE EXCITED FROM THE SUBSTRATE SIDE IN THE BACKWARD DIRECTION

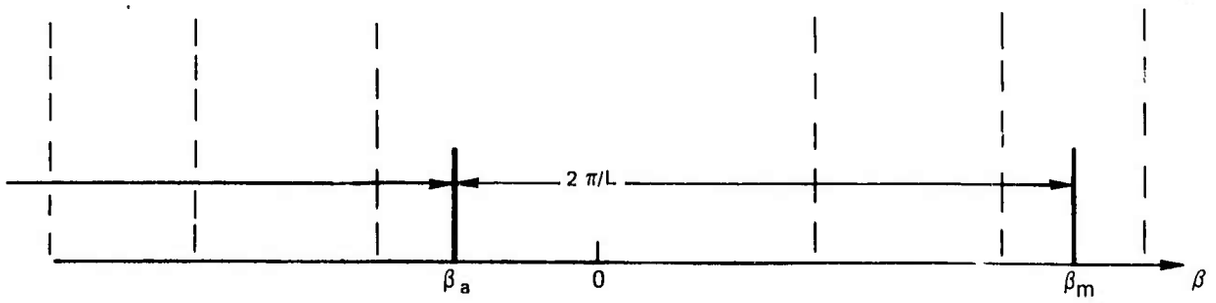

3.3.2 Phase Grating Fabrication Technique

3.3.2.1 Photomasks

From Fig. 18, we see that the grating periodicity L must be between 2.5 and 3.2 μm in order to achieve backward coupling. Several photomasks with L values in this range have been made at our laboratory. They are made by standard integrated circuit techniques with an overall reduction of about 2000X. The original artwork is first reduced by about 20X (the exact reduction depends on the grating periodicity required). This first reduction plate is then reduced by another 10X and at the same time stepped and repeated in order to cover the desired area. A final 10X reducation is done in the step and repeat machine to produce a square array of gratings, as shown in Fig. 19.

Since our automatic step and repeat machine has a fixed reduction of 10X, and is not able to make a step increment of a fractional mil, the first reduction procedure must be very carefully controlled to make an acceptable step and repeat master. Any error here will show up as a cumulative error in the final mask. That is, the error in the position of a groove (taking one edge of the grating as the reference) will be equal to the error in size of the step and repeat master pattern multiplied by the number of step distances to the groove in question.

Another serious error that can occur is in angular alignment of the step and repeat master to the x and y axes of the machine. This error would appear as jogs in the grating lines as well as the same cumulative error mentioned above.

Since our grating masks receive very rough treatment, we prefer not to use emulsion masks on our substrates. Instead, the pattern obtained as described above is contact printed on another plate containing a thin film of Shipley AZ1350 photoresist. An opaque layer of chromium is then rf sputter deposited on the plate. When the photoresist is removed in solvent it carriers away chromium deposited on the photoresist and leaves behind the chromium that lies directly on the glass. This then is our working plate.

3.3.2.2 Grating Fabrication

Since the coupled beam in most of our devices must travel in a direction parallel to one of the major cleavage planes, the first thing we must do to each substrate is locate these planes and somehow mark their directions. This is most easily done by removing a small piece of the substrate and breaking it. The major cleavage planes are then easily found by examination of the fragments. Once the direction is known, an edge of the substrate can be cleaved off and discarded.

The next operation is the sputter deposition of a thick layer of SiO_2 on the clean, chemo-mechanically polished substrate. This layer serves to protect the surface during subsequent procedures. Its thickness is not critical except that it must

FIG. 18

COUPLING ANGLE MEASURED FROM NORMAL AS A FUNCTION OF GRATING PERIOD FOR A 20 μm THICK GaAs THIN FILM WAVEGUIDE

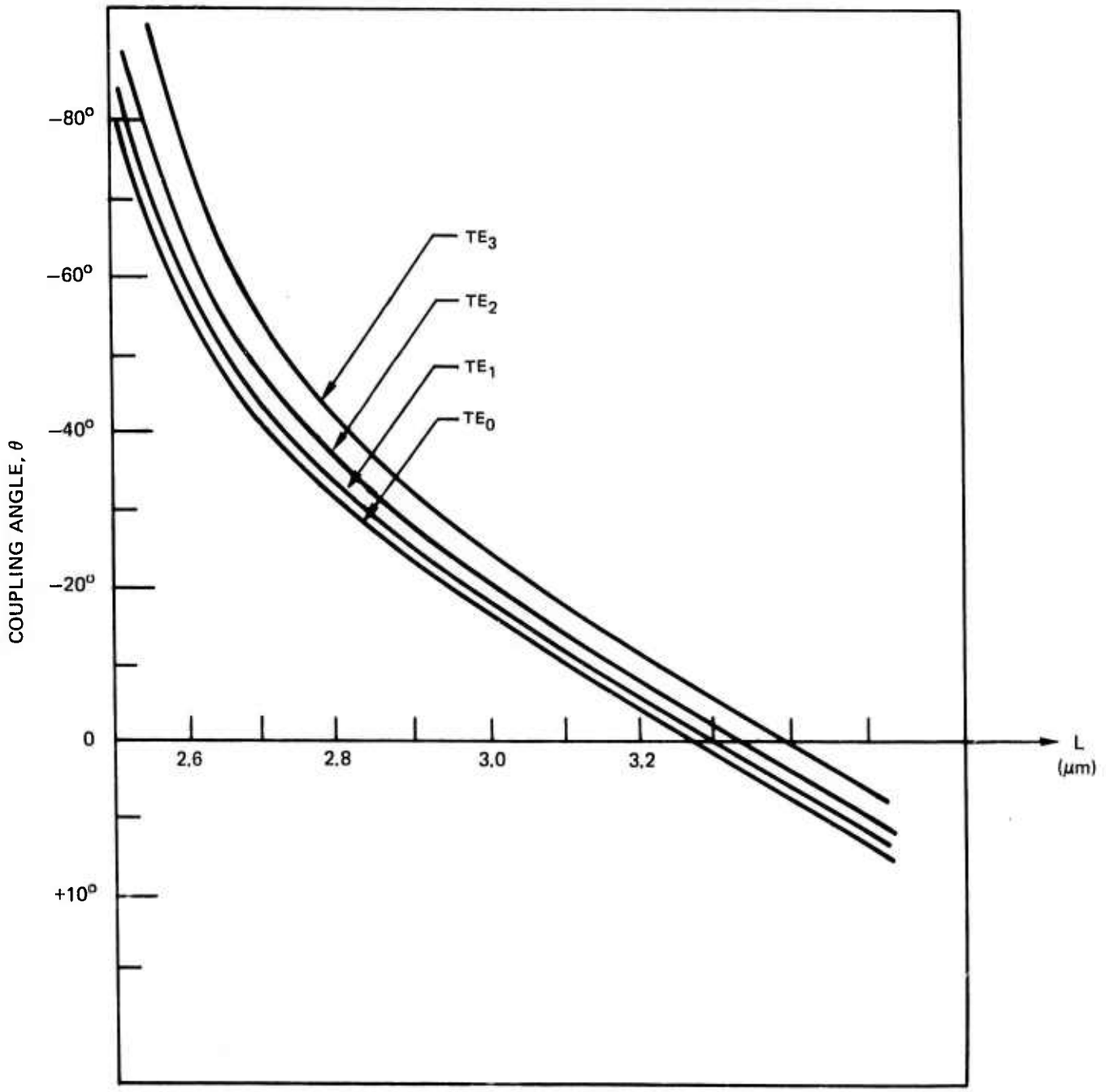

FIG. 19

A PHOTO MASK SHOWING ARRAY OF 3 mm x 3 mm GRATINGS HAVING L = 2.75 μm

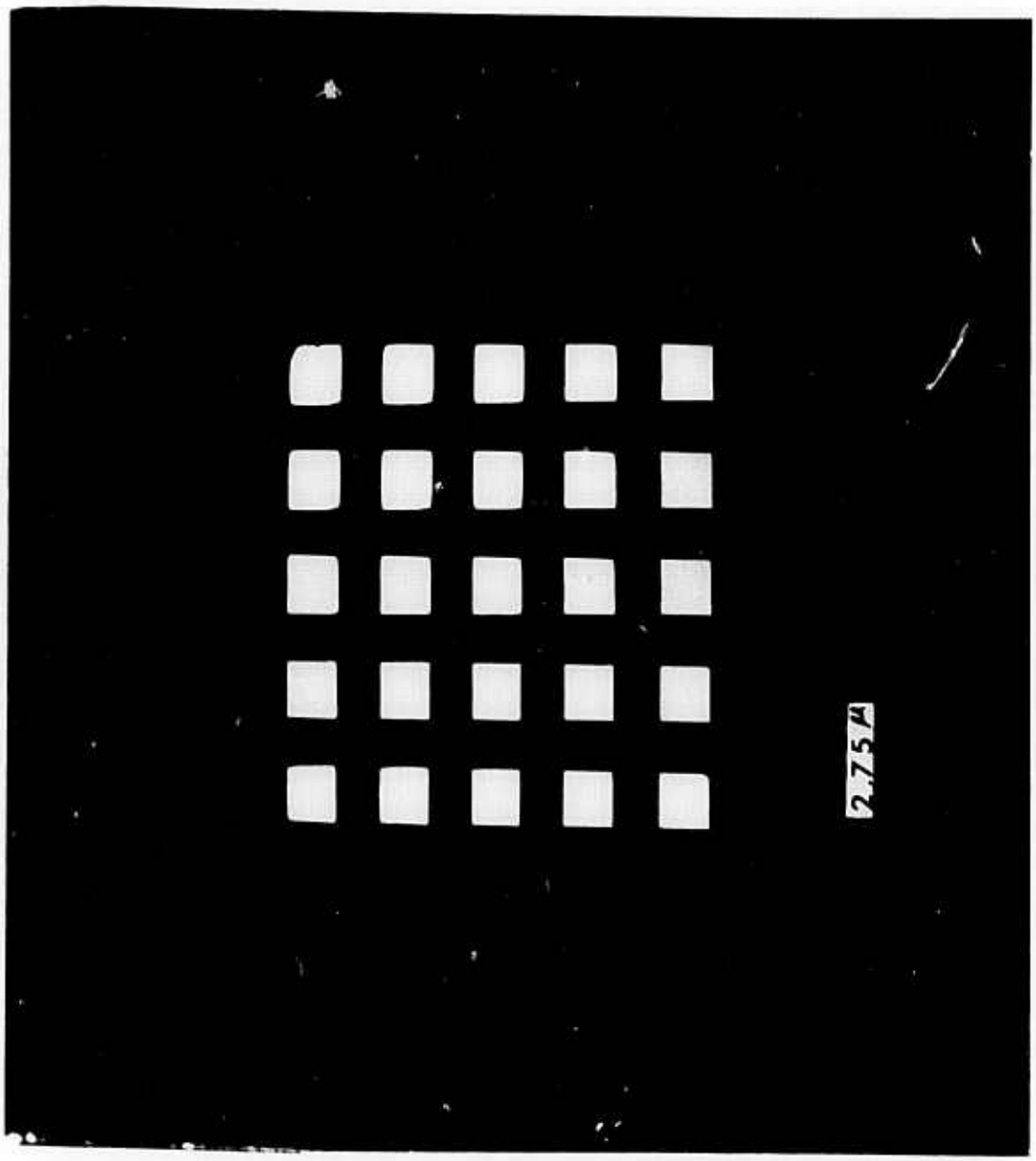

be very much thicker than the films actually used to form the grating and yet not so thick that it prevents obtaining intimate contact between the photomask and substrate.

A pair (or several pairs) of square windows is now opened in the protective oxide film using ordinary photoresist procedures. The sides of these pairs will be exactly colinear due to the nature of the mask making process and they should be as parallel to the cleaved edge of the substrate as possible.

The mask films (films used to mask and protect the grating ridges during sputter etching) are now deposited. They consist of first, a thin layer of SiO_2 and then 25 angstroms of chromium. After contact printing the grating pattern, using the thick oxide windows as alignment and position indicators, the substrate is ready for the grating formation procedure. This procedure is as follows:

1) The chromium film is sputter etched with the AZ1350 photoresist pattern acting as mask.

2) The thin oxide layer is chemically etched with the chromium film acting as mask.

3) Finally, the gallium arsenide substrate is sputter etched with the thin SiO_2 layer as the mask.

Two items should be noted at this point. Referring to the process described above, it can be seen that the only areas on the polished substrate (outside the gratings themselves) that are subject to sputter etching damage are where photo-resist defects in two separate steps coincide. These steps are the thick oxide window and the grating pattern definition. The other item is that the final groove depth is a function of the thickness of the thin oxide and of the relative sputtering rates of SiO_2 and GaAs. As an example, the thin oxide film on our 2.75 μm gratings is 0.2 μm thick and the relative sputtering rate is about 4:1 (GaAs:SiO_2) indicating that the maximum groove depth will be about 0.8 μm. Figure 20 is a Scanning Electron Microphotograph of a completed grating taken at 1000X and 5000X.

Figure 21 shows samples of the kinds of wafers that are now being prepared for this program. One or more sets of gratings that are optically in series are fabricated. Variable distance between multiple sets of gratings is used to aid in separating film-losses from grating losses. In addition one or more gratings is included for destructive examination (cleaving, staining and SEM work).

M921513–4

FIG. 20

A SCANNING ELECTRON MICROPHOTOGRAPH OF THE GRATING GROOVES ETCHED INTO GaAs THIN FILM

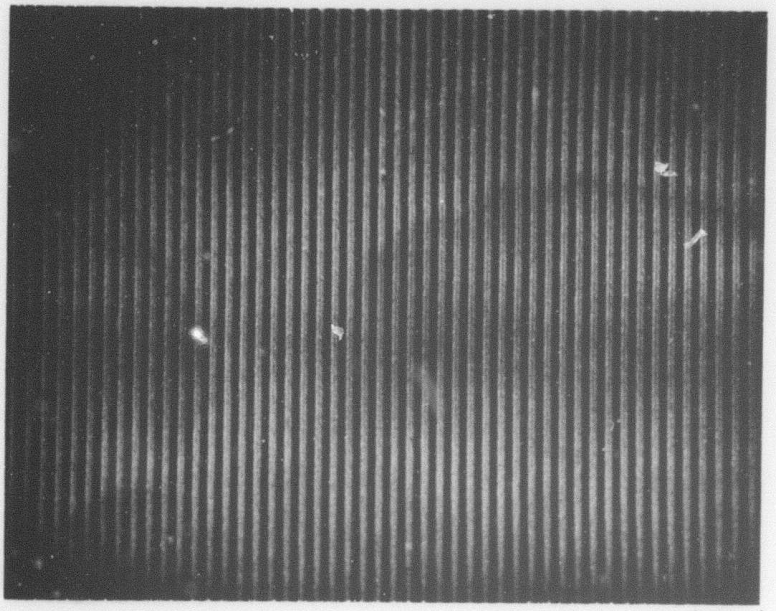

(a)

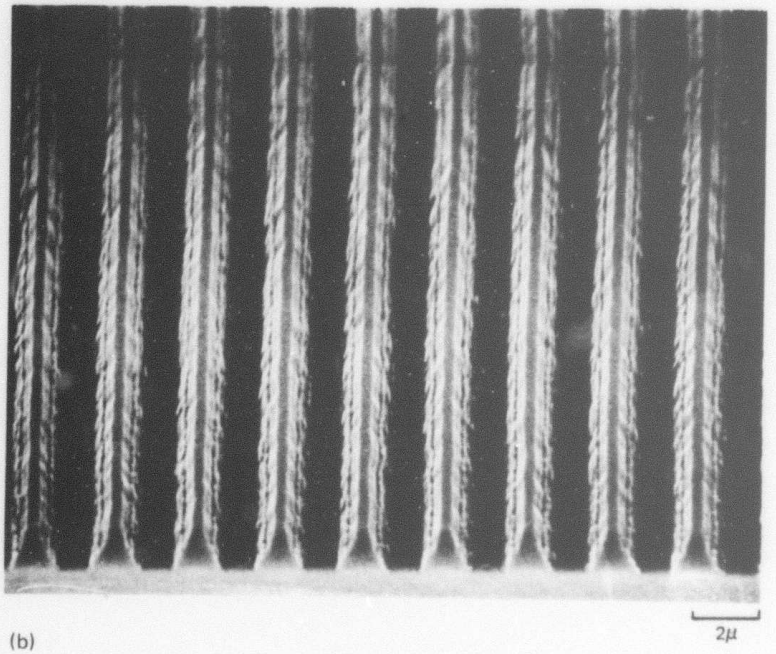

(b)

SAMPLES OF IR THIN FILM WAVEGUIDES

(a) FABRICATED BY CHEMO-MECHANICAL TECHNIQUE

(b) FABRICATED BY VAPOR-PHASE EPITAXY

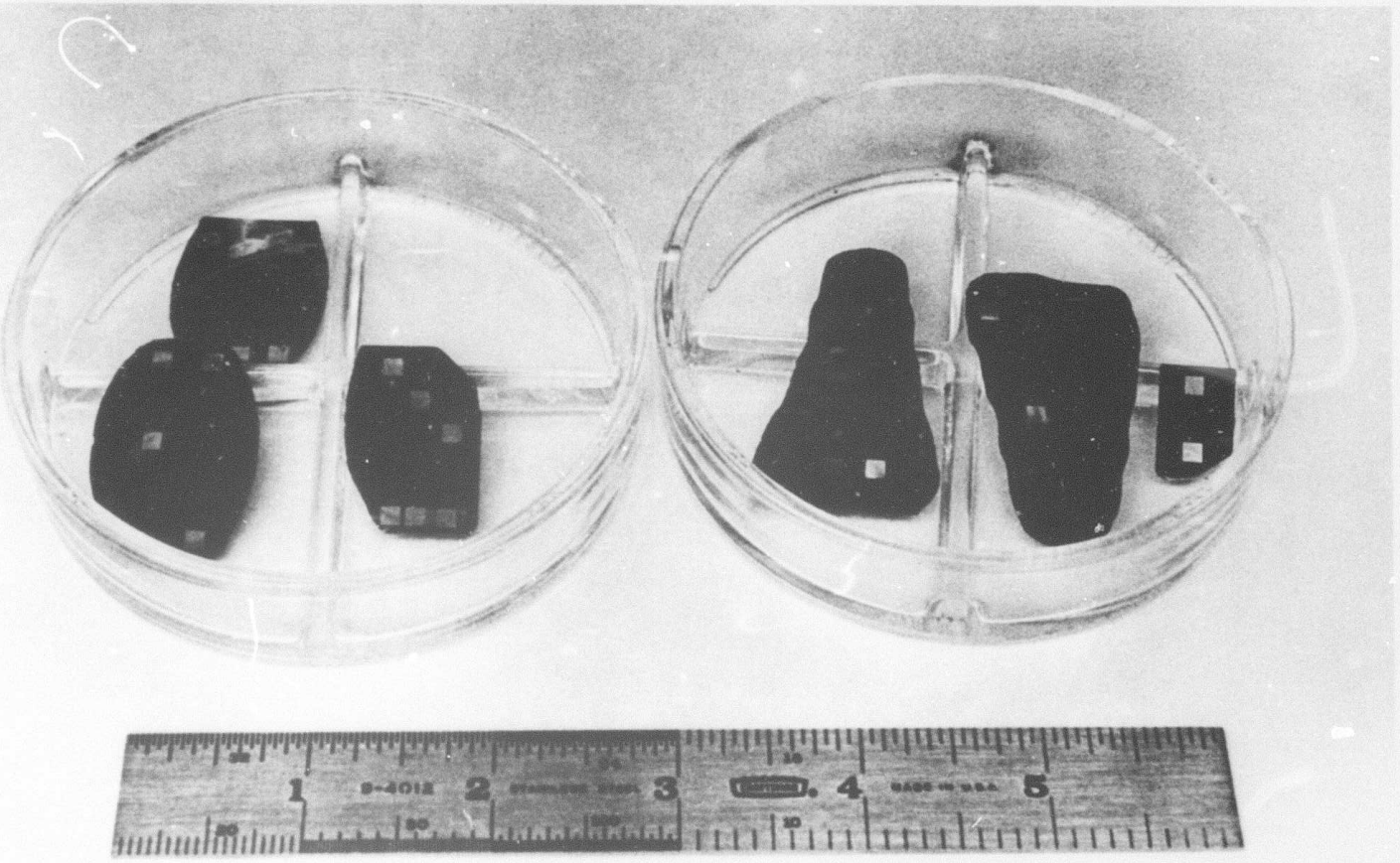

FIG. 21

4.0 MICROWAVE WAVEGUIDE STRUCTURES

4.1 Introduction

This section describes the work on the microwave aspects of the modulator for the 10 micron laser beam. The objective is to develop an efficient modulation scheme in the sense that minimum microwave power is required. This in turn implies that both the microwave energy and the laser beam be confined in a common waveguide. Confining the microwave power flow to the same waveguide as the infrared beam maximizes the obtainable electric fields required for the modulation process. Efficient interaction also requires that a synchronous condition exist between the rf wave and the optical wave.

A number of problems have been identified but they do not appear to be limiting ones. The potential problem areas include overcoming the microwave losses in the modulator section where the rf power is confined to a very small region. Recall that we are attempting to confine the rf power in a region which is approximately 1 mil high (the thickness of the gallium arsenide modulator) by 39 mils wide. This also raises an input matching problem with regards to obtaining wide bandwidth (ten percent). Finally, another problem is that of mounting the active material so that it can be used effectively with both the rf and the optical laser beam.

The last report (Ref. 5) discussed various aspects of this problem and described several approaches and techniques for the modulator. It was shown that a long narrow gap ridge waveguide would be suitable for the microwave modulation structure. Through the use of a simplified model for the ridged waveguide, the attenuation in the gallium arsenide filled ridge waveguide was estimated and from this was estimated the power required to drive the rf modulator. The attenuation was estimated to be about 1 dB/cm and the power level was estimated to be approximately 40 watts. The suggested structure for the final modulator was a transversely fed ridge waveguide. In this concept each half wavelength or possibly full wavelength section of the modulator is driven separately but in phase through a power divider. This will produce a standing wave along the modulator but the bandwidth will correspond to that of a single driven section. By properly leading the ridge waveguide the synchronous condition can be satisfied.

The work during this period was concentrated on experimentally determining the parameters of the ridge waveguide with both air and gallium arsenide as the filling medium. The experimental work and results will be presented in the following sections and then a description of the first test modulator will be given.

4.2 Experimental

The electrical characteristics of the ridge waveguide of the dimensions required for the thin film optical modulator are not readily available since there has not

been a practical need for microwave circuits with these dimensions. The requirement of an efficient modulator, efficient in the sense that a minimum amount of rf power is required, makes it necessary to know in detail the characteristics of the narrow ridge waveguides, the associated parasitic reactances, and as well, the location of appropriate reference planes. With this information it becomes possible to apply established microwave techniques to achieve not only efficient operation but optimum microwave bandwidth as well.

Before proceeding with the experimental work an approximate analysis of the ridge waveguide will be given to show the range of frequencies over which it can be used. The cross-sectional parameters of the ridge waveguide are shown in Fig. 22. It can be readily shown that the characteristic impedance of the ridge waveguide is equal to $z_o = 1/vC$ where C is the equivalent capacitance per unit length and v is the phase velocity. Then using the transverse resonant condition for establishing the cutoff frequency of the waveguide (Ref. 13) with an expression for Y (as defined in Fig. 22)

$$Y = \frac{1}{j377h'\tan\left(\frac{\omega}{v_o}h\right)} = j\frac{\omega C}{2} \tag{14}$$

one finally obtains from that condition an expression for the product of h x h', (using the small angle approximation for $\tan\theta$)

$$hh' \simeq \frac{2z_o v_o^2}{377\omega_{co}^2} \tag{15}$$

where ω_{co} is the cutoff frequency of the waveguide. For an optimum choice of dimensions, h equals h', the following relationship for h is obtained

$$h = \sqrt{\frac{2z_o}{377}}\frac{\lambda_{co}}{2\pi}. \tag{16}$$

now expressed as a function of the desired cutoff wavelength for the propagating structure. For example, h = .19" corresponds to a cutoff frequency of 5 GHz. This cutoff frequency is well below the desired operating frequency of 10 GHz and therefore is a useful nondispersive structure for our purposes. In the above it was assumed that the gap region was adjusted so that z_o was equal to 50 ohms. For lower impedances even smaller values of h can be used effectively.

The first experiments with the ridge waveguide were done in the structure shown in Fig. 23. The overall waveguide dimensions were .5 inches wide by .25 inches high. A 50 ohm miniature line was connected at each end of the ridge section as shown so that transmission or reflection measurements could be made. Furthermore, one of the coaxial connections could be withdrawn so that an open circuit condition could be established at that end of the ridge section. This structure allows us, in addition,

CROSS SECTION PARAMETERS FOR NARROW GAP RIDGE WAVEGUIDE

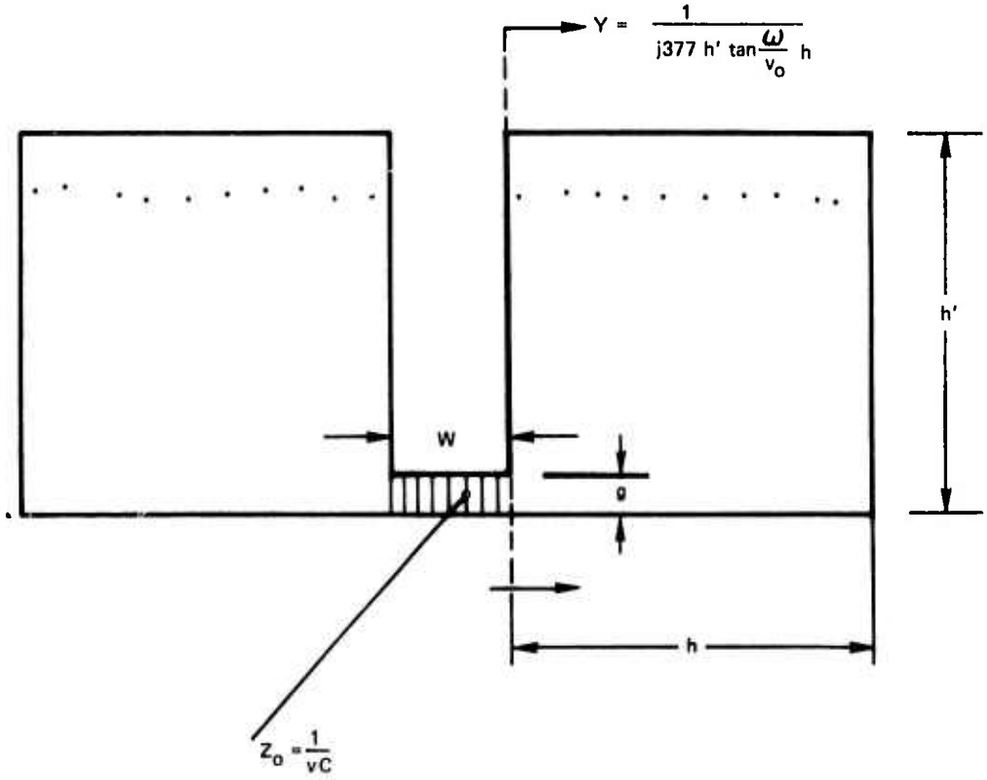

FIG. 23

RIDGE WAVEGUIDE TEST SECTION

a) TEST SECTION

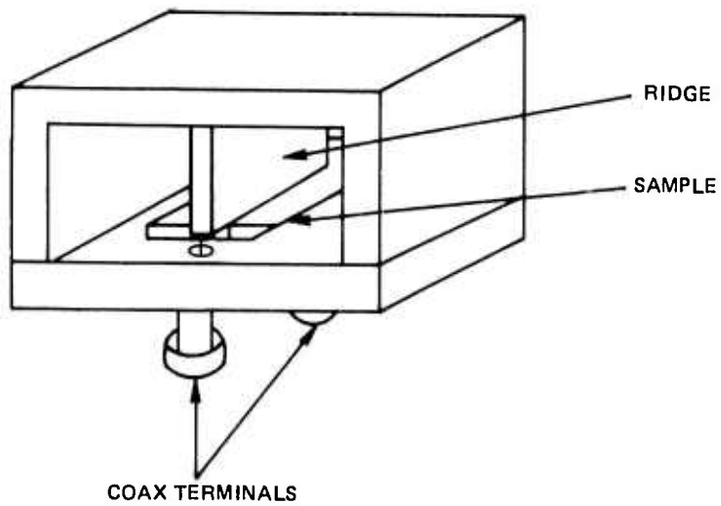

b) DETAILS OF RIDGE SECTION

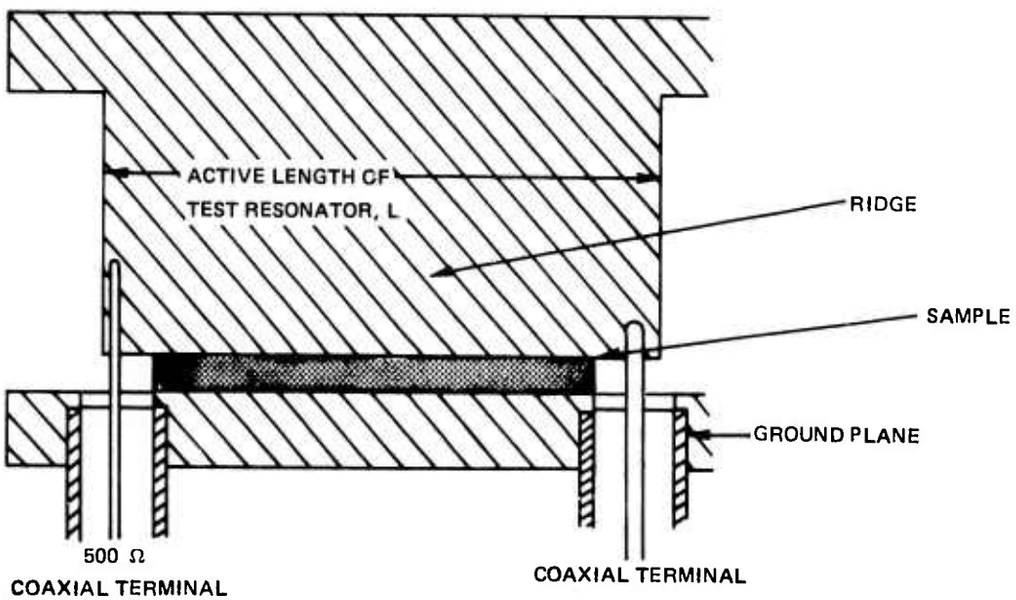

to make measurements either with or without gallium arsenide sandwiched between the ridge and the ground plane, and also permits the gap size of the ridge section to be varied. The variable gap height experiments have been performed with the gallium arsenide strip removed so as to obtain design information on air filled sections. These sections would be used for impedance matching from the 50 ohm input into the ridge waveguide terminals. The adjacent 50 ohm coax input lines were made small, its center conductor is 20 mils in diameter; thus the coaxial input line was made more compatible in size to the dimensions of the ridge. This approach minimizes parasitic reactances.

In order to fully characterize the ridge transmission line and the parasitics associated with the junctions to the coax lines it was necessary to establish reference planes for the measurements and the circuit model. The locations are shown in Fig. 24. One reference plane AA is established at the end of the coax line at the surface of the ground plane. The second reference plane is established at the point at which the coax center conductor is in contact with the ridge waveguide. With these reference planes established, elements can be introduced in the equivalent circuit shown in Fig. 24(b) which consists of the uniform line of length L and the arbitrary two-terminal networks T.

For various conditions of the ridge transmission line two basic measurements were made from 8 to 12 GHz with a sweep generator and a Hewlett Packard network analyzer. One measurement made was the input impedance with the 50 ohm termination at the end of the line and the second measurement was the input impedance with the coax termination at the end of the line removed. Because of the fact that the cutoff frequency is very low, even in the air filled gap, one can assume that the velocity of propagation is essentially that of free space. Thus, by noting resonant frequencies and comparing them to the values expected if there were no parasitic reactances, and by measuring input resistances at resonances, one can deduce the parasitic reactances associated with the junctions, the attenuation coefficients, and the characteristic impedance of the air lines for various heights. With these results and further measurements on the GaAs filled gap we have established the characteristic impedance of this structure and its effective velocity of propagation. For this set of measurements the length of the test section was 4 cm. In supplementary experiments a section of the ridge was removed so that two open circuit sections were formed. In this case there was a transmission line 1.26 cm in length on one side and another transmission line 1.72 cm in length on the other side.

From the input impedance data in the form of Smith chart plots from the network analyzer, it was found that lumped circuit elements in the network labeled T in Fig. 24 could be represented as shown in Fig. 25. The transition network contains two capacitors, one in series and one in shunt. The values of these elements are tabulated in Table IV for gaps ranging from 1 mil up to 8 mils in height. These values are approximate in as much as the attenuation coefficients of the transmission lines were not taken into account in reducing the data. The absence of an inductor may seem incorrect; however, a series capacitor properly accounts for the observed impedance variation from 8 to 12 GHz. Values for the characteristic impedance of the

FIG. 24

REFERENCE PLANES FOR RIDGE WAVEGUIDE

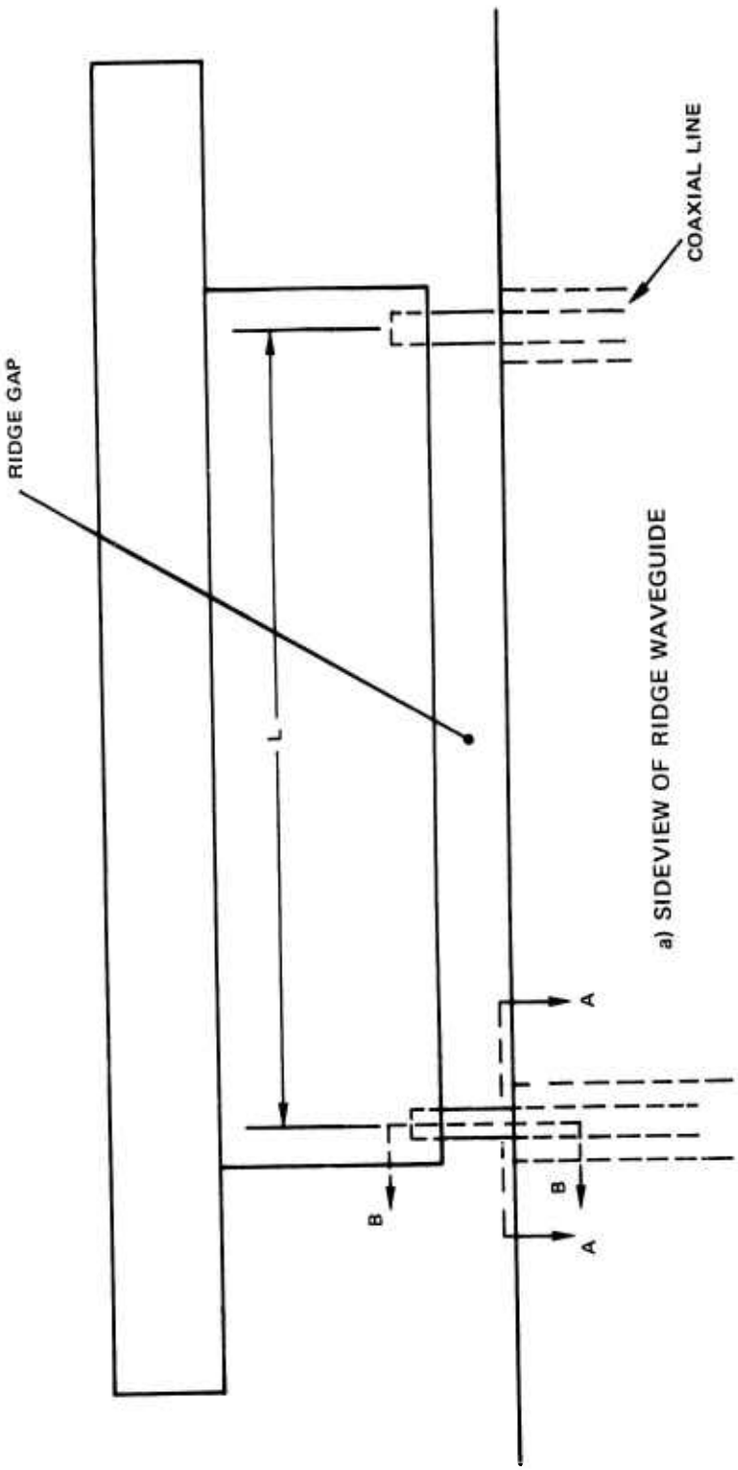

a) SIDEVIEW OF RIDGE WAVEGUIDE

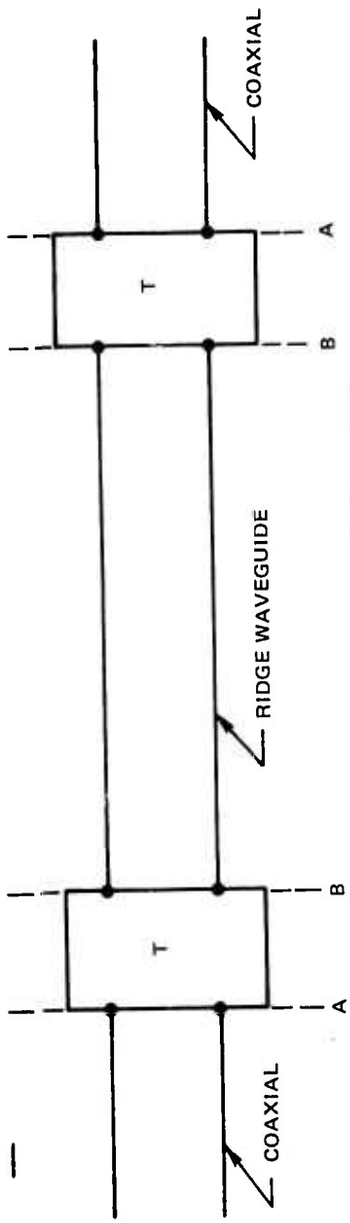

b) GENERAL EQUIVALENT CIRCUIT

FIG. 25

SPECIFIC EQUIVALENT CIRCUIT

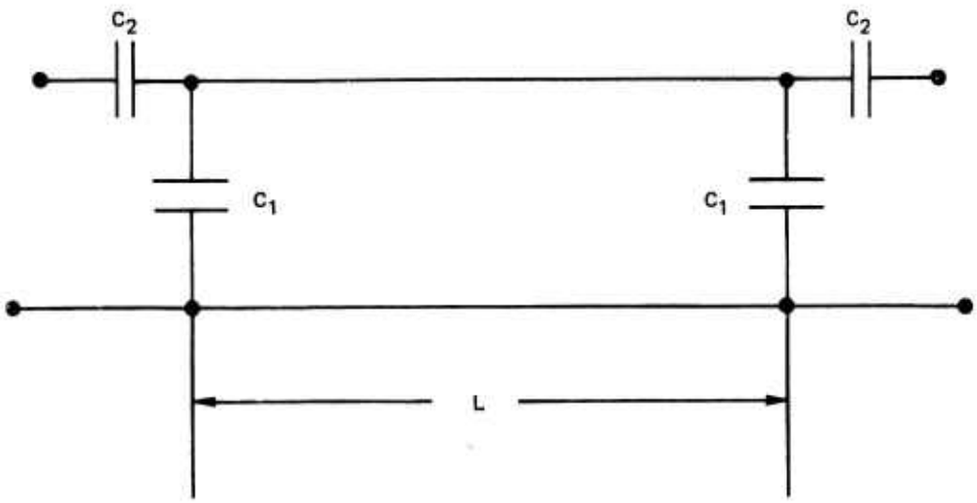

TABLE IV

Values of Parasitic Elements for Transition from Miniature Coax to Narrow Ridge Waveguide

Gap	C_1	C_2
.001	.17 pF	11.4 pF
.002	.08	5
.003	.06	3
.005	.05	1.5
.007	.02	1
.008	.01	.7

lines were determined by using the fact that, whenever the transmission line is an odd multiple of a quarter wavelength it serves as an impedance transformer from the 50 ohm termination to the measured input impedance. Thus the simple expression, $R = z_L^2/50$, can be used to compute the characteristic impedance of the transmission line. The attenuation can be determined from the open circuited lines by measuring input impedance at resonance, i.e., when the transmission line is a multiple of a half wavelength, by applying the transmission line equations with losses. The results are shown in Fig. 26 which contains curves of the characteristic impedance and attenuation (dB/cm) for various gap spacings. For the range of air gaps from one mil to 8 mils the characteristic impedance varies from 13 ohms up to 55 ohms.

From similar measurements with the gallium arsenide filling the gap it was possible to obtain the characteristic impedance of the transmission line corresponding closely to the actual modulator. A single data point shown in Fig. 26, for GaAs is 5 ohms. The corresponding attenuation is roughly 0.5 dB per centimeter. At this point an estimate can be made of the guide wavelength in the gallium arsenide filled ridge waveguide. In general the ratio of the characteristic impedance for dielectric filled waveguide to the air filled waveguide is the same as the ratio of the velocities of propagation. From the characteristic impedance measurements this turns out to be a ratio 1/2.7. Additional measurements of resonant frequencies made with the shorter open circuit sections described earlier were also used to determine this same ratio of velocities. These measurements yielded a value of 1/3.1 which compares reasonably well with the characteristic impedance ratios. More accurate determinations of z_o, λ_g and the parasitics will be carried out, if required, using an optimization technique which accounts for the parasitics reactances and attenuation simultaneously. We might note here that the synchronous condition between the microwave waves and the laser beam requires that the effective velocity of the microwave be c/3.3. Thus microwave techniques will have to be applied to the ridge waveguide structure to further slow the wave down. The attenuation will also change accordingly. This modification will be discussed shortly.

A photograph of the two section ridge and the base plate are shown in Fig. 27. The vertical posts on the base plate are used to align the ridge structure. Indicated on the photographs are the positions for the input and output coaxial lines and the sockets into which the center conductors fit on the ridge section. Also shown is one of the 1 mil gallium arsenide strips which was placed under the ridge which is .039 inches wide.

Two Smith chart plots taken with the network analyzer for the two lengths of ridges are shown in Fig. 28. The resonant frequencies are indicated. The data reduction consisted of first selecting possible values for the number of half wavelengths present at the resonant frequencies, computing the corresponding ratios of free space wavelength to guide wavelength, and then selecting the value common to the various lengths. Of particular interest in Fig. 28 are the values of input impedance for the open circuited lines at resonance, approximately 50 ohms and 125

EXPERIMENTAL PARAMETERS FOR NARROW GAP RIDGE WAVEGUIDE

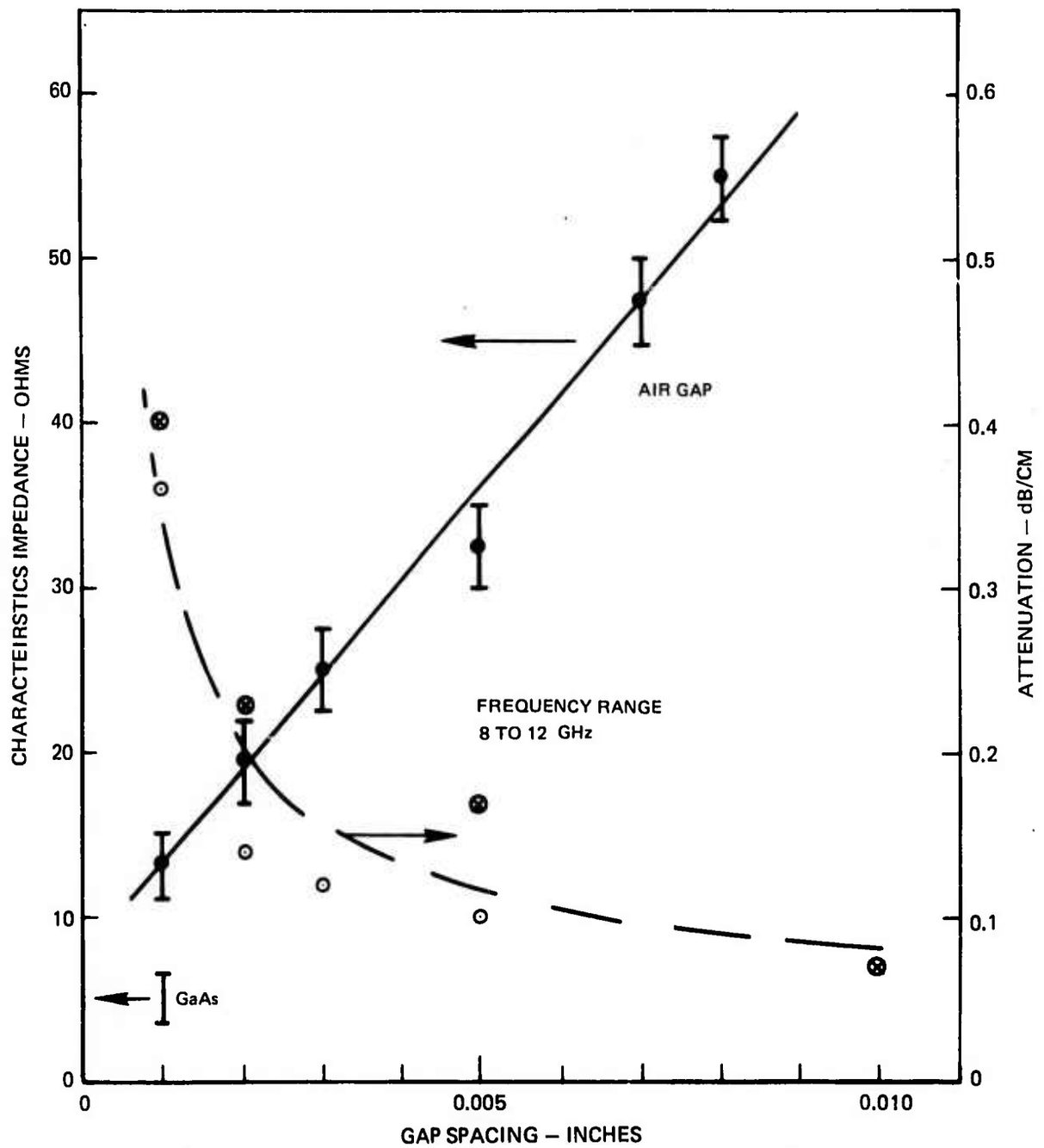

FIG. 27

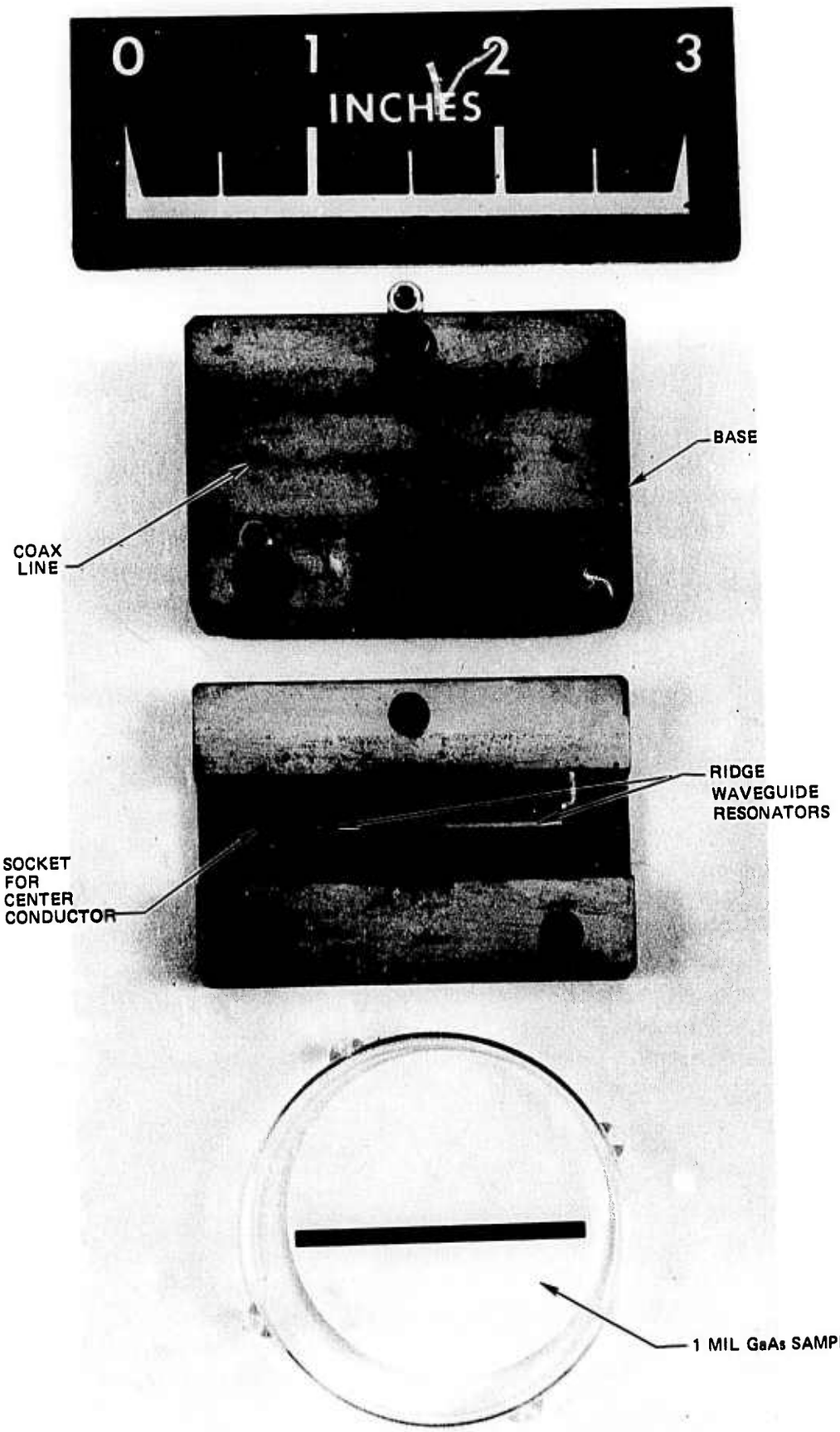
0
1
2
3
INCHES
BASE
COAX LINE
RIDGE WAVEGUIDE RESONATORS
SOCKET FOR CENTER CONDUCTOR
1 MIL GaAs SAMPLE

FIG. 28

INPUT IMPEDANCES OF OPEN CIRCUIT GaAs FILED RIDGE WAVEGUIDE

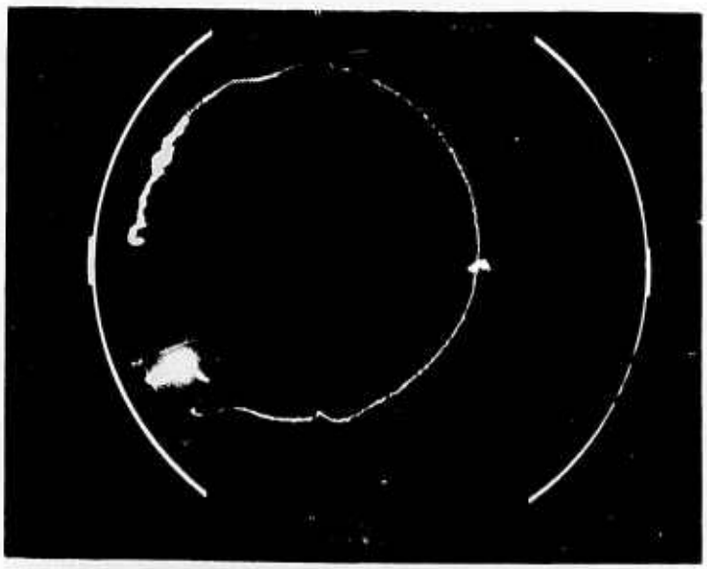

GaAs IN NOTCHED RIDGE II INPUT

a) 1.25 CM

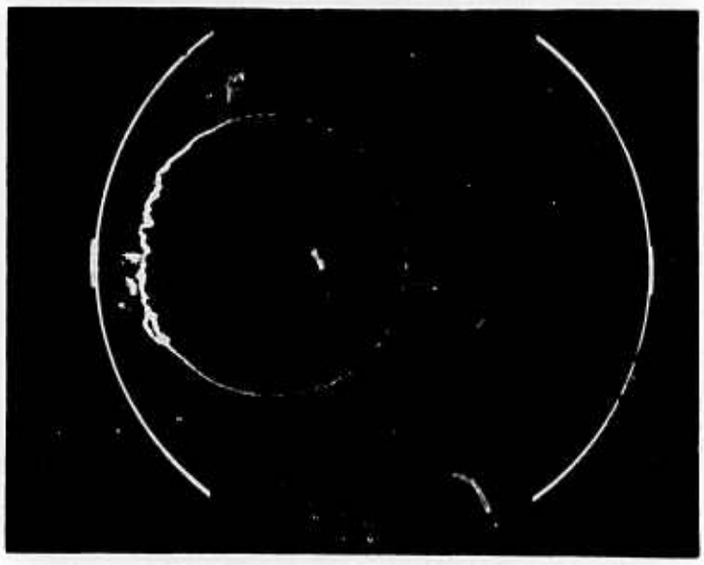

0.001 GaAs IN NOTCHED RIDGE I INPUT

b) 1.72 CM

ohms. These results indicate what levels of impedance one will have to match into if the ridge sections of the waveguide are to be used as open circuited resonantors. This operation would provide only narrow band modulation in a demonstration of modulation at microwave frequency.

4.3 Optical/Microwave Thin Film Modulator Configuration-First Model

Based on results collected so far on the narrow gap ridge waveguide filled with gallium arsenide a design was selected as the first model of the microwave modulator for the present program. This model will be used to demonstrate the microwave modulation efficiently without regard to broadband operation. In the last report (Ref. 5) the transverse feed technique was analyzed and it was shown that a cell which is essentially 1 wavelength long would provide the desired bandwidth. The structure being fabricated is shown in Fig. 29. It consists of two open circuit transmission lines driven at a common point from a single source. The use of a single drive point facilitates the tuning adjustments at this stage of the experiments. It becomes much more difficult to simultaneously adjust four or five input terminals. Each section is one wavelength long. The figure shows the location of the gallium arsenide slab, the input terminals and the approximate locations of the optical coupling gratings. Also shown in the ridge are notches to slow the wave down so that the synchronous condition will exist between the microwave and the laser beam. It is convenient that the microwave velocity of propagation is greater than that of the optical beam and therefore the simple notch can be used to slow the wave down to the desired value. The experiments with this structure will permit microwave measurements on the actual thin film material that will be used for the modulator. The information gained from tuning and matching will then be used to fabricate the multiple cell unit with parallel feeds.

FIG. 29

SKETCH OF RESONANT MODULATOR

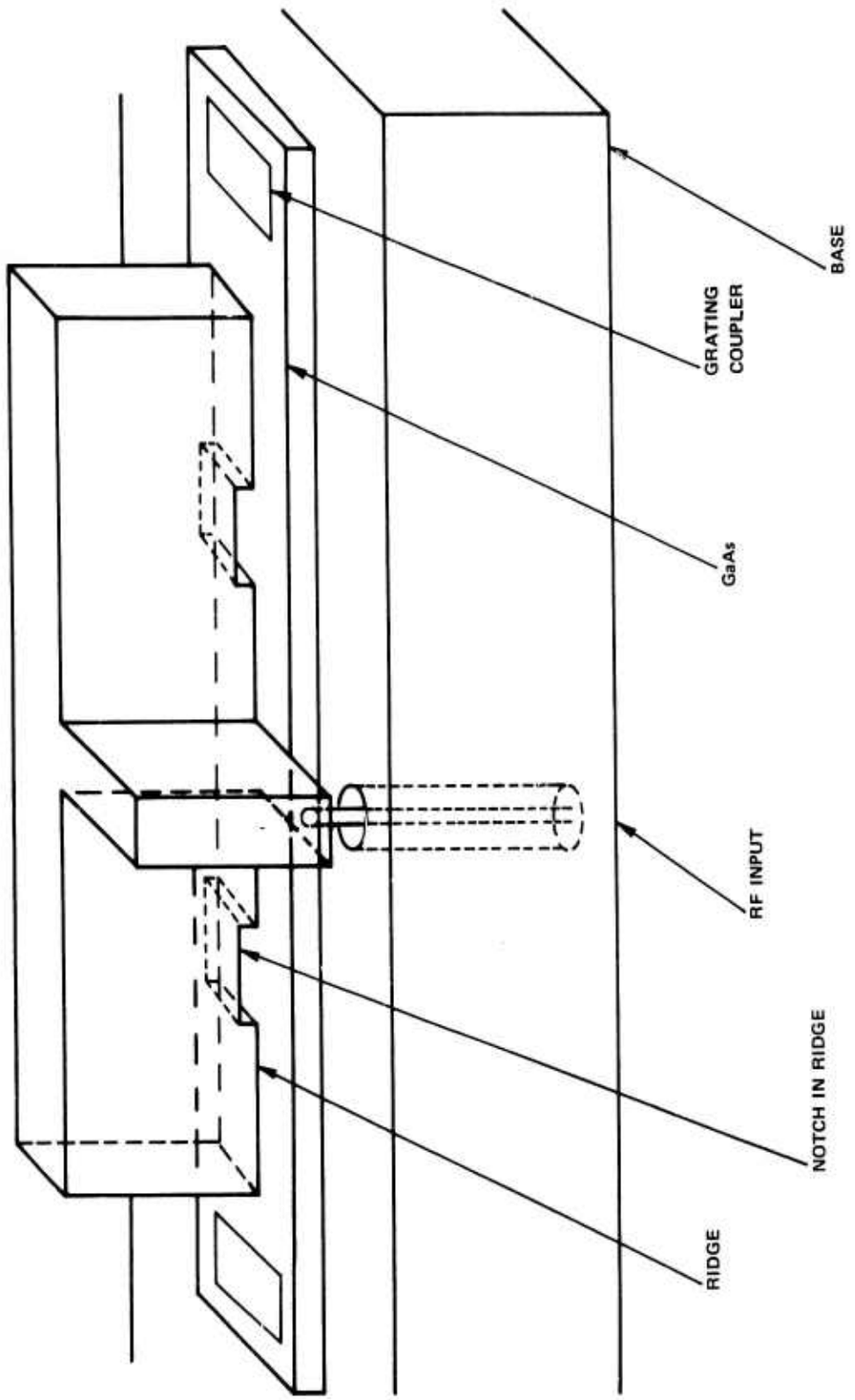

REFERENCES

1. P. K. Cheo, et al, Appl. Optics, 12, 500 (1973).

2. P. K. Cheo, Appl. Phys. Letters, 22, 241 (1973).

3. P. K. Cheo, Appl. Phys. Letters, 23, No. 8, 15 October 1973.

4. P. K. Cheo, T. M. Reeder and J. L. Swindal, UARL Technical Report AFAL-TR-73-120, May 1973.

5. P. K. Cheo, UARL Interim Report, ONR-N00014-73-C-0087 Under ARPA Order 1860, March 1973.

6. K. Ogawa, W. S. C. Chang, B. L. Sopori and F. L. Rosenbaum, IEEE J. Quant. Elect., QE-9, 29 (1973).

7. F. K. Reinhart, D. F. Nelson and J. McKenna, Phys. Rev., 177, 1208 (1969).

8. F. K. Reinhart and B. I. Miller, Appl. Phys. Letters, 20, 36 (1972).

9. I. P. Kaminow, Appl. Phys. Letters, 7, 123 (1965); F. K. Reinhart, J. Appl. Phys., 39, 3426 (1968).

10. I. P. Kaminow and E. H. Turner, Proc. IEEE, 54, 1374 (1966).

11. R. L. Abrams and D. A. Pinnow, J. Appl. Phys., 41, 2765 (1970).

12. P. K. Tien and R. Ulrich, J. Opt. Soc. Am., 50, 1325 (1970).

13. S. B. Cohn, Proc. IRE, 35, 783-788, August 1947.